

FORCED HYDRAULIC JUMP ON ARTIFICIALLY ROUGHENED BEDS

**A THESIS SUBMITTED TO
THE GRADUATE SCHOOL OF NATURAL AND APPLIED SCIENCES
OF
MIDDLE EAST TECHNICAL UNIVERSITY**

BY

ÇAĞDAŞ ŞİMŞEK

**IN PARTIAL FULFILLMENT OF THE REQUIREMENTS
FOR
THE DEGREE OF MASTER OF SCIENCE**

**IN
CIVIL ENGINEERING**

DECEMBER 2006

Approval of the Graduate School of Natural and Applied Sciences

Prof. Dr. Canan ÖZGEN
Director

I certify that this thesis satisfies all the requirements as a thesis for the degree of Master of Science.

Prof. Dr. Güney ÖZCEBE
Head of Department

This is to certify that we have read this thesis and that in our opinion it is fully adequate, in scope and quality, as a thesis for the degree of Master of Science.

Assoc. Prof. Dr. Nuray TOKYAY
Supervisor

Examining Committee Members

Prof. Dr. Mustafa GÖĞÜŞ (METU, CE) _____

Assoc. Prof. Dr. Nuray TOKYAY (METU, CE) _____

Prof. Dr. Tülay ÖZBEK (Gazi Üniv., İnşaat Müh.) _____

Assoc. Prof. Dr. İsmail AYDIN (METU, CE) _____

Asst. Prof. Dr. Burcu Altan SAKARYA (METU, CE) _____

I hereby declare that all information in this document has been obtained and presented in accordance with academic rules and ethical conduct. I furthermore declare that, as required by these rules and conduct, I have fully cited and referenced all material and results that are not original to this work.

Name, Last Name: Çağdaş Şimşek

Signature: 

ABSTRACT

FORCED HYDRAULIC JUMP ON ARTIFICIALLY ROUGHENED BEDS

ŞİMŞEK, Çağdaş

M. Sc., Department of Civil Engineering

Supervisor: Assoc. Prof. Dr. Nuray Denli TOKYAY

December 2006, 88 Pages

In the scope of the study, prismatic roughness elements with different longitudinal spacing and arrangements have been tested in a rectangular flume in order to reveal their effects on fundamental characteristics of a hydraulic jump. Two basic roughness types with altering arrangements have been tested. Roughness elements of the first type extends through the channel width against the flow with varying *length* and *pitch* ratios for different arrangements. The second type is of staggered essence and produced by piecing the roughness elements defined in the initial type into three parts which are equal in length. The doublet formed from the pieces on the sides is shifted to the consequent row to make two successive roughness rows encapsulate the channel span completely. Staggered roughness type is formed with the repetition of this arrangement along the flume. Independent of their type and arrangement, the entirety of roughness elements are embedded in the channel bed in order to avoid their protuberance into the flow, based on the presumption that the crests of the roughness elements levelled with the channel inlet would be less exposed to caving effects of flow than the protruding elements.

In the study, influence of the proposed roughness elements on the fundamental engineering concerns as the length, height (tail water depth) and energy dissipation capacity of hydraulic jumps has been questioned in the light of empirical work and related literature on forced and smooth hydraulic jumps.

At the final stage of the study, it was concluded that both strip and staggered roughness have positive effects on the characteristics of hydraulic jump given above. 3-7% more energy dissipation was observed in jumps on rough beds compared to classical hydraulic jumps. For tailwater dept reduction, whereas strip roughness provided 5-13%, staggered roughness led to 7-15% tailwater depth reduction compared to classical hydraulic jump. While strip roughness reduced jump length around 40%, 35-55% reduction was observed with staggered roughness when compared to classical hydraulic jump.

KEYWORDS: Hydraulic Jump, Energy Dissipation, Non-protruding Prismatic Roughness, Rough Bed, Roughness Arrangement

ÖZ

YAPAY PÜRÜZLÜLÜKLÜ AÇIK KANALLARDA KONTROLLÜ HİDROLİK SIÇRAMA

ŞİMŞEK, Çağdaş

Yüksek Lisans, İnşaat Mühendisliği Bölümü

Tez Danışmanı: Doç. Dr. Nuray Denli TOKYAY

Aralık 2006, 88 Sayfa

Bu çalışma kapsamında, kanal boylamına farklı aralıklarla ve dizilimlerle yerleştirilen prizmatik pürüzlülük tipleri, hidrolik sıçramanın temel özelliklerine etkilerini ortaya koymak amacıyla dikdörtgen kesitli bir kanalda test edilmiştir. Dizilimleri değişen iki ana pürüzlülük türü sınanmıştır. İlk türdeki pürüzlülük elemanları, değişken *uzunluk* ve *diş yüksekliği* oranlarıyla kanalın en kesitini tümünden geçerek, kanal boyunca akıntıya karşı yerleştirilmiştir. İkinci türse şaşırtmalı bir yapıda oluşturulmuş ve ilk türde tanımlanmış pürüzlülük elemanlarının üç eşit parçaya bölünmesiyle üretilmiştir. Kenarlarda bulunan iki parçadan oluşturulan ikili, birbirini takip eden iki pürüzlülük sırasının tüm kanal aralığını kapsayabilmesi için bir sonraki sıraya kaydırılmıştır. Şaşırtmalı pürüzlülük türü, bu dizilimin kanal boyunca tekrarlanmasıyla meydana gelmiştir. Tepe düzlemleri kanal ağzının taban kotuyla aynı olan pürüzlülük elemanlarının akıntıya girenlere oranla daha az kavitasyona (oyulmaya) maruz kalacağı varsayımına dayanarak, türlerinden ve dizilimlerinden bağımsız olarak pürüzlülük elemanların tamamı akıntıya müdahalelerini engellemek üzere kanal yatağının içine gömülmüştür.

Çalışmada, önerilen pürüzlülük elemanlarının, sıçramanın uzunluğu, yüksekliği (aşağı akım derinliği) ve enerji sönümlenme kapasitesi gibi temel mühendislik kaygılarına etkisi, ampirik çalışmalar ve kontrollü ve klasik hidrolik sıçrama ile ilgili literatürdeki çalışmalar ışığında irdelendi.

Çalışmanın sonunda, şerit biçimli ve şaşırtmalı pürüzlülüğün, hidrolik sıçramanın yukarıda belirtilen özelliklerinde olumlu etkilerinin olduğu görülmüştür. Pürüzlendirilmiş açık kanallarda oluşan hidrolik sıçramada, klasik hidrolik sıçramaya göre %3-7 arası daha fazla enerji sönümlenmiştir. Aşağı akım derinliğinde ise, şerit tipi pürüzlülük klasik hidrolik sıçramaya göre %5-13 arası, şaşırtmalı tipse %7-15 arası daha az aşağı akım derinliği sağlamıştır. Şerit pürüzlülük, hidrolik sıçrama uzunluğunu klasik hidrolik sıçramaya göre %40 civarında azaltırken, bu oran şaşırtmalı pürüzlülükte %35-55 arasında gerçekleşmiştir.

ANAHTAR KELİMELER: Hidrolik Sıçrama, Enerji Sönümlenmesi, Gömülü Prizmatik Pürüzlülük, Pürüzlü Yatak, Pürüzlülük Dizilimi

ACKNOWLEDGEMENTS

*"buğün yağmur bir kadın saçdır
yeryüzüne dökülen
upuzun ince ince
karanlık kokulu..."*

First, I would like to thank to my thesis advisor Assoc. Prof. Nuray Tokyay who, with her great patience and support, guided me through this tough path and life-changing experience. It has been a pleasure and privilege to study with you.

Furthermore, I wish to express my gratitude to the staffs of the Engineering Faculty and Department of Civil Engineering at the Middle East Technical University who provided me with material and emotional support, time and belief.

I would like to thank to Sema Seçkin and Berat Yoldaş who have given me support in completing my laboratory sessions with their joyful presence, support and encouragement.

I would like to express my thanks to Şule Şahin, Talia Ekin Tokyay, Onur Açar, Mehmet Bozok and Yusuf Ziya Pamukçu for the love, support and encouragement they have provided me with their presence in my life.

I also present my special thanks to my tutors and friends in the Department of Sociology at METU. They always encouraged me in completing my study.

I would like to express my profuse gratitude to my aunt Mukadder Gökmen, her husband İbrahim Gökmen and my cousins Gamze and Gökben Gökmen, who have never made me feel away from home.

Finally; thank you Meral, for being a friend rather than a mother to me; Hasan, a father like you makes life “an easier task” for me; and ıđdem; more than a sister, you are joy of my life.

TABLE OF CONTENTS

ABSTRACT	iv
ÖZ	vi
ACKNOWLEDGEMENTS	viii
TABLE OF CONTENTS	x
LIST OF FIGURES	xii
LIST OF TABLES	xv
LIST OF SYMBOLS	xvi

CHAPTER

1. INTRODUCTION	1
1.1 Introduction	1
1.2 Literature Review	4
1.3 Aspirations	12
1.4 Outline of the Text	13
2. WHAT IS A HYDRAULIC JUMP?	14
2.1 Fundamentals of Hydraulic Jump	14
2.1.1 Conjugate Depths in Classical Jump	14
2.1.2 Sequent Depths for a Flow under a Sluice Gate	19
2.1.3 Energy Dissipation between the Upstream and Downstream Sections	20
2.1.4 Length of Jump	24
2.1.5 Free Surface Profile and Pressure Distribution	27
2.1.6 Velocity Distribution along the Jump	29
2.2 Jump Taxonomy regarding the Supercritical Condition and Surface Profile	32
2.3 Definitions and Parameters Employed in the Present Study	33

3. EXPERIMENTAL SETUP AND PROCEDURES	37
3.1 Description of the Experimental Setup	37
3.2 Features of the Roughness Elements Used	40
3.3 Calibration of the V-notch Weir	40
3.4 Experimental Apparatus	42
3.5 Experimental Procedures	42
4. DISCUSSION OF RESULTS	46
4.1 Overall Assessment of Experimental Runs	46
4.2 Energy Dissipation at the Jump Upstream	53
4.3 Energy Dissipation along the Channel	56
4.4 Gain in Energy Dissipation	59
4.5 Depth Ratio	61
4.6 Reduction in Tailwater Depth	63
4.7 Length of Hydraulic Jump	65
4.8 Reduction in Length of Jump	69
5. CONCLUSIONS	73
5.1 Overall Assessment of Experimental Runs	73
REFERENCES	75
APPENDICES	80
A. COLLECTED AND COMPUTED DATA	80
B. FORMER EMPIRICAL WORK	83
C. LABCARD MANAGEMENT AND PROBE CALIBRATION	86

LIST OF FIGURES

Figure 1.1: Definition sketch for hydraulic jump over roughened bed (Negm, 2002)	10
Figure 2.1: A typical hydraulic jump formed on a smooth bed	16
Figure 2.2: Integrated bed shear force as denoted by the solid line (Ohtsu and Yasuda, 1990)	18
Figure 2.3: Free flow under a typical sluice gate (Lin et al. 2002)	19
Figure 2.4: Hydraulic jump profile and associated specific energy diagram	22
Figure 2.5: Variation of relative energy loss with incoming Froude number - Modified- (Rajaratnam and Hurtig, 2000)	23
Figure 2.6: Variation of L/y_1 scale with F_1 (Ead and Rajaratnam, 2002)	25
Figure 2.7: Correlation between the subcritical length parameter and F_1 (USBR, 1955)	26
Figure 2.8: Flow profiles of Bakhmeteff and Matzke (1936)	28
Figure 2.9: Definition sketch of Rajaratnam and Subramanya's (1968) profile ...	29
Figure 2.10: Velocity profiles in classical hydraulic jump for $F_1=4.30$ (Hager and Bremen, 1989)	30
Figure 2.11: Velocity profile at a single section (Rajaratnam, 1965)	31
Figure 2.12: An undular jump profile (Ohtsu et al., 2003)	32
Figure 2.13: Length parameters of the recent study [I]	33
Figure 2.14: Length parameters of the recent study [II]	34
Figure 2.15: Length parameters of the recent study [III]	34
Figure 3.1: Schematic Representation of the Experimental Setup --Modified- (Evcimen, 2005)	38
Figure 3.2: Dimensioning of the pressure tank (Evcimen, 2005)	39

Figure 3.3: General view of the pressure tank	39
Figure 3.4: Wave probe and point gauge	42
Figure 3.5: Wave probe calibration formula obtained in one of the runs	43
Figure 3.6: A screenshot of the Labcard software	44
Figure 4.1: A view of steady jump ($F_1=9.65$) [I]	47
Figure 4.2: A view of choppy jump ($F_1=9.65$) [II]	47
Figure 4.3: Weak jump formation	48
Figure 4.4: A view of jump for strip roughness with $w/L=4$, $w/Z=6$, $F_0=5.08$, $F_1=3.28$	48
Figure 4.5: A view of jump over a strip roughness of $w/L=4$, $w/Z=6$, $F_0=5.08$, $F_1=4.02$	49
Figure 4.6: Steady jump [Reflection of the flasher is dimmed]	49
Figure 4.7: Burst shooting of a choppy jump	50
Figure 4.8: Bucket effect	51
Figure 4.9: Bucket effect initiation at 2 nd and 3 rd rows	52
Figure 4.10: Separation observed at 4 th and 5 th rows	52
Figure 4.11A: Sluice gate with a streamlined lip	54
Figure 4.11B: Length parameters of pre-jump energy loss	54
Figure 4.12: Relative energy loss in the channel prior to jump for rough and smooth beds	55
Figure 4.13: Energy dissipation with strip roughness versus F_1 for different length ratios	57
Figure 4.14: Energy dissipation rate for staggered roughness with respect to F_1	57
Figure 4.15: Comparison of the data obtained in this study with the previous ones	58
Figure 4.16: Energy dissipation rates in smooth channels and in channels with strip and staggered roughness versus F_1	58
Figure 4.17: Percent gain in energy dissipation for different length and depth ratios for beds of strip and staggered roughness	60
Figure 4.18A: Variation of depth ratio with supercritical Froude number for different length and pitch ratios in strip roughness arrangements	61

Figure 4.18B: Variation of depth ratio with supercritical Froude number for different length and pitch ratios in staggered roughness arrangements	62
Figure 4.19A: Percent tailwater depth reduction in beds with strip roughness	63
Figure 4.19B: Tailwater reduction in the flume with supercritical Froude number for varying length and pitch ratios in beds with staggered roughness	64
Figure 4.20A: L_j/y_2^* versus F_1 in beds with strip roughness	66
Figure 4.20B: L_j/y_2^* versus F_1 in beds with staggered roughness	67
Figure 4.21: Sketch of an undular hydraulic jump (Chanson and Montes, 1995)	68
Figure 4.22A: Overall L_j/y_2^* trend for strip roughness	68
Figure 4.22B: Overall L_j/y_2^* trend for staggered roughness	69
Figure 4.23A: Percent length reduction factor for strip roughness	70
Figure 4.23B: Percent length reduction factor for staggered roughness	71

LIST OF TABLES

TABLE AA: Tabular form of data collected in the present study	80
TABLE BA: Evcimen's data for $w/Z=4$ and $w/Z=6.67$ (Evcimen, 2005)	83
TABLE BB: Ayanlar's data for $t=10$ (Ayanlar, 2004)	84
TABLE BC: Data of Ead and Rajaratnam for $t=1.3$ and $t=2.2$ (Ead and Rajaratnam, 2002)	85
TABLE BD: Data of USBR for length parameter (USBR, 1955)	85

LIST OF SYMBOLS

a or b	Opening height of a sluice gate
b or B	Channel width
C_c	Contraction coefficient
D	Tailwater depth reduction factor
E_1	Specific energy at the upstream section
E_2	Specific energy at the downstream section
E_L	Loss in energy per unit weight of the flow
F_1	Froude number of supercritical flow
F_2	Froude number of subcritical flow
g	Gravitational acceleration
G_{ED}	Gain in energy dissipation
H	Head measured above the V-notch
H_L	Head loss
L_j	Length of jump
L_J^* or L_s	Length of jump in a smooth bed
L_r	Length of a jump on a rough bed
q	Discharge per unit width for a given section
Q	Volumetric discharge
R_1	Upstream Reynolds number
R_L	Jump length reduction factor
s	Lateral spacing between roughness elements installed in staggered arrangement
S_f	Integrated dimensionless bed shear force per unit width
u_1	Supercritical flow velocity
u_2	Subcritical flow velocity
u_m	Maximum cross-sectional velocity

V	Average flow velocity
w	Longitudinal spacing between two roughness elements in successive rows from the internal edges
w_h	Longitudinal spacing between two roughness elements in successive rows from the centres
x_{vc}	Longitudinal distance taken from the gate to Vena Contracta
y_1	Flow depth at the jump toe
y_2	Flow depth at the end of the jump
y_2^*	Conjugate depth of a classical hydraulic jump
y_{vc}	Flow depth at Vena Contracta
Y^*	Sequent depth ratio
Z	Height of the roughness element
α	Notch angle for a triangular weir
B	Momentum correction coefficient
ΔE	Energy loss in a jump formed in a rough bed
ΔE^*	Energy loss in a classical jump
Δx	Longitudinal distance from Vena Contracta to jump toe
γ	Unit weight of water
δ	Height of the boundary layer
δ_1	Flow depth where cross-sectional velocity equals $u_m/2$
λ_j	Relative length of a jump
ν	Kinematic viscosity of water
ρ	Mass density of water
\bar{S}	Non-dimensional bottom shear force
τ_0	Bed shear stress

CHAPTER I

INTRODUCTION

1.1. Introduction

Chow defines a hydraulic jump as the abrupt change of flow in the direction of flow in an open channel flow under certain conditions, where flowing stream passes from supercritical flow to subcritical flow (*Chow, 1959*). However, some of the recent work defines this change as a transitory process where the supercritical state transforms into the subcritical in a finite distance or a “transition zone.” Throughout this transition phenomenon, the supercritical shallow-water flows dissipate mechanical energy and advance on a subcritical state (*Hákonardóttir et al., 2003*).

Although first described by Leonardo da Vinci in the 16th Century, the history of scientific and engineering concerns on hydraulic jump phenomenon extends through 1820's with the leading studies of Italian Giorgio Bidone (1781-1839) who imposed constant energy head across the hydraulic jump. In 1838, Jean Bapiste Belanger (1790-1874) correctly utilised the momentum equation for the prediction of pre-jump and post-jump depths, namely the sequent depths. Though Henri Bazin (1829-1917) empirically verified Belanger's concept with limited observation, it was not until 1910 and the following decade when Arnold Gibson (1878-1959) presented experiments that corroborated the analytical work of Belanger. Belanger's concept of “sequent depths” obtained final recognition by the 1916 paper of the American Karl R. Kennison (1886-1977) whose closure verified data of several different sources as stated by Hager (*1990*).

In an open channel flow, transition from the rapid state to tranquil state is characterised by the development of large-scale turbulence, surface waves, energy dissipation and air entrainment (*Chanson and Montes, 1995*). The rapid state is an indispensable outcome of flows passing through and over hydraulic structures as spillways, sluice gates and weirs where a mass of water collected in an upstream reservoir is released. The excess potential energy stored in accumulated upstream water evolves into kinetic energy, i.e. gains high velocities, while passing, in the form of flow, through these structures. This excess energy should be dissipated in order to prevent downstream sections from scouring and hydraulic structures' themselves from failure. The reason for utilising the energy dissipation unit at the downstream of a hydraulic storage structure is to ensure the safety of the overall structure being subjected [sic] to tremendous dynamic loading through operation (*Negm, 2000*).

Besides their energy dissipation function, hydraulic jumps are commonly used in the operation of flow-measurement flumes to increase efficiency, mixing chemicals or air to streams, desalination of sea water, sedimentation of solid particles in high velocity flows, chlorination of domestic water sustaining systems and aeration of streams polluted by bio-degradable wastes.

Normally, all hydraulic structures should have a form of energy dissipation structure as a stilling basin where hydraulic jump takes place. This dissipation structure should be designed to confirm the hydraulic jump formation over to avoid the expected damage to the floor of the overall structure. The length of the hydraulic jump is mostly taken as a design parameter or as an indicator of the length of the paved downstream section, i.e. the stilling basin. From the engineering standpoint, the length of the stilling basin should be both efficient in energy dissipation and economical in fiscal terms. For the most economical stilling basin design, its length should be kept as short as possible (*Negm, 2002*). The performance or efficiency of any stilling basin is usually assessed in terms of characteristics of the jump it allocates (*Negm, 2000*). Pavement is applied to the basin in order to secure it against the scouring effects of the through-flow with high kinetic energy. A basin is rarely designed to confine the mature length, i.e. the entire length where flow profiles fully formed, since such a basin would be too long and expensive (*Chow, 1959*).

Another important parameter is the elevation of the banks that confine the jump in the basin. The height of the sidewalls should be as low as possible to be economical. Low downstream depth of jump would reduce the cost pertaining to both pre-construction excavation and sidewall height.

The stability of jump is a further parameter of crucial importance. In the horizontal channels, the locus of the hydraulic jump below a sluice gate moves considerably when the tailwater elevation is altered. From the designer's point of view, the jump should remain as stable as possible in a horizontal apron (*Ohtsu and Yasuda, 1994*).

In order to satisfy these principle criteria, devices as sills, baffle blocks, endsills, roughness elements, screens, riprap aprons, riprap outlet basins, roller buckets, flip buckets are installed into the spillway or basin in structures and laboratory models. This study focuses on the stilling basins with rough beds. Rajaratnam (*1968*) was the first researcher who conducted a systematic experimental study on hydraulic jump under the effect of rough bed (*Negm, 2000*). These roughness elements are mounted into stilling basins in different arrangements and versions.

The flow conditions downstream of the jump are deduced from the momentum and continuity equations and the upstream flow conditions (*Chanson and Montes, 1995*). The upstream Froude number, which is the ratio of upstream flow velocity to celerity of water at the same section, is the chief criterion designating the conditions of the tailwater depth and jump type. In basins where the design discharge generates flows with very high Froude numbers at the upstream section, hydraulic jump loses its economical advantages over other methods since the tailwater depth increases excessively.

Among many others, the study of Ead and Rajaratnam (*2002*), too, indicated that rough beds have positive effects in the reduction of the jump length and tailwater depth. The interaction of flow with the corrugated rough bed is asserted to be the main reason for the enhancement of bed shear stresses. Moreover, the study illustrated clearly that the integrated shear stress at the boundary layer of the roughened bed is ten times greater than that on a smooth bed. The main concern with jumps on rough beds, according to Ead and Rajaratnam, however, is that the roughness elements protruding into flow at the upstream section of the basin

might be subjected to excessive cavitation and erosion due to the supercritical flow with high velocities. In such a case, the jump would move downstream sections reaching the unprotected streambed which would threaten the overall stability of the structure. But a roughened bed with roughness elements whose crests are levelled with the inlet bottom, the roughness elements would not be protruding into the flow and thus be faced with less caving effects compared to protruding roughness elements.

Air may be counted among agents employed against cavitation. Mainly due to the oscillating breaking front at the toe of the jump, air is entrained into jumps as bubbles making the hydraulic jump a bubbly two-phase flow (Liu, et al., 2004). Peterka (1953) recognised the air leak as a possible method of reducing cavitation damage. He set up a design standard for the required air concentration in high-speed flow to counter cavitation damage. With a minimum air concentration, between 5 and 8 %, observations indicated that damage due to bubble collapse could be inhibited (Hager, 2003).

1.2. Literature Review

Rajaratnam (1968) seems to be the one who conducted the first systematic experimental study on jumps in roughened basins. *Equivalent relative roughness height* as a basin parameter varied between 0.02 and 0.43 while Froude number as the flow parameter was kept in the interval of 3 to 10 in his experimental runs. The depths ratio was concluded to be the dependent variable of both the supercritical Froude number and the *relative roughness height*. He also reported that the length of the jump on roughened bed halved that of a smooth jump with a significant increase in energy dissipation.

It was Perry et al. (1969) who focused on transverse ribs as a roughening agent for the investigation of flow in the turbulent boundary layer. The authors formed two categorisations, namely the k-type and d-type roughness in the former of which the chief determinant in the roughness function was the height of the roughness. In the latter type, namely the d-type roughness, the foremost determinants of the

influence of roughness on flow are the boundary layer thickness of flow, pipe diameter in closed-conduit flows and channel height in open channel flows.

Leutheusser and Schiller (1975) carried out experiments downstream of a sluice gate in a horizontal and roughened rectangular open channel flume to inquire the development of supercritical channel flow and performance of hydraulic jumps with fully-developed inflow. Tests were run on four different types of rough beds covering the entire width and length of the channel. The authors reported that conventional non-dimensional jump length parameter decreased with an increase in relative roughness. In their experimental study it is shown that with an increase in relative roughness; there arises a tendency for steeper upstream roller faces, increased sequent depths ratio, and low Froude-number jumps to assume wavy-surface profiles. Roughness elements have been stated to accelerate the upstream-flow development and hence engender and ease the formation of hydraulic jumps.

Hughes and Flack (1983) investigated the effect of various roughness designs on the characteristics of a hydraulic jump in a stilling basin. The authors also set Froude number as a flow variable to investigate the outcome of roughness designs under different flow conditions. Seven different roughness designs including square-sectioned parallel bars positioned normal to the flow and closely packed gravel bonded to a Perspex plate were investigated under varying inflow characteristics. For gravel models, a hypothetical surface plane coinciding with the crests of the strip elements is assumed. Both the extent of roughness and Froude number of supercritical flow were found to be effective in the reduction of the tailwater depth and jump length.

Tani (1987) concluded that for regularly-spaced rib-type roughness elements, the transitory pitch ratio is 4 for the changeover from k-type with higher pitch ratios to d-type with lower pitch ratios, where pitch ratio is defined as the ratio of the distance between two successive ribs to the rib height.

Hager and Bremen (1989) investigated the influence of wall friction on the sequent depths ratio. Their theoretical and empirical study indicated that there always exists a slight difference between the depths ratio obtained by the Belanger equation and the laboratory models. The authors proposed a limit for

the scaling deviation between the laboratory data and theoretical computations, which is 5%. The ± 5 % deviation between the laboratory data and theoretical values is proposed to be a result of scaling effect due to reduced-down model dimensions. Deviations exceeding this limit are articulated to be the outcome of the effect of fluid viscosity. The authors also proposed an equation in order to test whether the model is subject to a scaling discrepancy.

Mohamed Ali (1991) studied hydraulic jump downstream of low-head irrigation channels with rough beds under different flow conditions to obtain the optimum length for the roughened bed section in both engineering and economical terms. Laboratory experiments indicated that cubic roughness elements reduce the jump length. He concluded that the variation in the ratio of the length of roughened section of the bed to the roughness height for cubic roughness elements outputs an optimal value for this ratio, L_{rb}/z , where the jump length minimises. For $L_{rb}/z = 28$, the effective length of jump, which is the ratio of length of jump to the supercritical depth, drops remarkably. This reduction ranges from 27.4% to 67.4% for initial Froude numbers ranging from 10 to 4 which indicates that the increase in the supercritical Froude number results in longer hydraulic jumps for cubically roughened beds.

Garimella and Eibeck (1992) investigated the separation and reattachment behaviour of flow over an array of protruding roughness elements mounted on the bottom wall of a rectangular water channel using laser doppler velocimetry. The authors have tested three roughness arrangements with three distinct streamwise spacing, L_s/B , 2.2, 4.3 and 6.5, where L_s stands for the longitudinal spacing between elements and B refers to the height of a single roughness element. The authors introduced the concept of *array shear* to demarcate the region where the flow is retarded by the resistance of the array. They have also reported flow separation at the initiating rows of the roughness elements. In their study, the confining or interacting nature of the flow encapsulated in the cavities between the roughness elements is established as a function of the element spacing. Moreover, the authors have reported that the reattachment length downstream of an element varies in between 4 and 1.5 element-heights which decreases both with increased Reynolds numbers and decreased roughness height. The cavity flow at the smallest spacing, i.e. 2.2, the authors asserted, has been largely confined

in the cavities. Yet, it was unsteady and it alternated between intense and confined vertical activity, and strong interaction with the outer flow via the downwashing of the bypass flow in the cavity. The horseshoe vortices formed in front of the initial rows of the elements are reported to form in front of the higher row elements, too, with increased streamwise spacing, i.e. 4.3 and 6.5. Again, the vortices in between the elements with larger streamwise spacing have been reported to reattach in the cavity with a resulting intense interaction between the cavity and channel flow. These reattachment lengths, i.e. 4 and 1.5 element heights, have been reported to be in sharp contrast with those proposed for the two-dimensional models in the literature reaching 11 to 15 rib heights.

Krogstad and Antonia (1999) studied turbulent boundary layers and questioned the k-type and d-type boundary typology. They also studied the differentiated flow-mixing effects of different roughness types even though flows passing over them possess approximately identical velocity profiles in the vertical section. These observations, the authors assert, strongly challenge the conventional concept that roughness effects are confined to a thin layer in the vicinity of the wall surface. Authors, in this way, criticised the classical boundary layer theory which separates the overall flow section into two distinct sub-layers, namely the boundary layer and the channel flow which have nearly nil interaction. The experimental evidence, as the authors reported, suggested that the surface geometry significantly affects the turbulent characteristics of the flow, even though the roughness elements in question are selected among those which have nominally the same effect on the mean velocity. For two very different roughness elements leading to approximately identical flow-velocity function, significant differences can be discerned on Reynold's stresses; $\rho \overline{uv}$ and, especially, $\rho \overline{v^2}$.

Negm (2000) studied the hydraulic performance of rectangular and radial stilling basins, where the latter stand for the diverging channels. He analysed experimental results of a series of experiments conducted in a laboratory flume where basins with or without sills have been tested under both free and submerged flows. He concluded that radial basins were more efficient than rectangular ones in engineering terms. Moreover, he reported that the length of the jump dropped significantly and more energy was dissipated in the former type. The use of radial basins also reduced the sequent depth ratio when

compared to rectangular basins. Radial basins had also lower values for the coefficient of discharge in the discharge equation. The use of roughness in both basin types had significant positive effects on energy dissipation and reduction of jump length.

Negm (2000) has also drawn conclusions on the studies of Abdelsalam et al. (1985, 1986, 1987), Hammad et al. (1988), Mohamed Ali (1991), Negm et al. (1993), Alhamid and Negm (1996) and Negm et al. (1999) on regularly roughened beds. In the overall context, the following outcomes from the outlines of the above studies have been drawn. 12% is the most efficient intensity for roughness elements with square cross-sectional area installed as a series of strips with equal spacing transverse to the flow. 13% is the most efficient intensity for hexagonal cross-sectional area placed in a staggered manner. This reaches to 15% for hexagonal cross-sectioned strips arranged as strips in series transverse to the flow which indicates three-dimensional roughness in hexagonal cross-section is more efficient in terms of hydraulic concerns. 16% is the most efficient intensity for roughness elements in circular cross-sectional area mounted in a staggered arrangement. This value rises to 20% when the arrangement is transformed into strips against the flow, which illustrates once more that three-dimensional roughness reduces the required efficient intensity. 40% intensity is required for the most efficient design for the roughness elements with semi-circular cross-sectional area arranged as strips in series located against the flow. It might be predicted that the structure of the lattermost alternative resembles that of the corrugated beds.

Tachie et al. (2000) question the consent on the hypothesis which assumes that a k-type roughness only influences the flow structure in the immediate vicinity of the flow structure in turbulent flows with some new measurements of the mean velocity profile in a shallow open channel flow for three different types of roughness elements and in a hydraulically smooth bed. They report that there are reasonable grounds to assess a roughness encapsulated in the turbulent boundary layer can modify the velocity profile even outside the roughness sub-layer. The conclusion which draws that bed surface effects influence the flow structure in the outer region of the boundary layer contradicts the wall similarity hypothesis. Hence, it has implications which necessitate coping with the challenging task of

incorporating the specific effects of different roughness elements on the near-wall flows. Another observation the authors made was that the extension of the rough-wall effects through the outer flow region and penetration of the turbulence intensity deep into the wall region suggest that it is appreciable to study rough-wall flows under elevated turbulence intensities for better assessment of the interactions between the inner and outer regions of the turbulent boundary layer. In other words, increased turbulence intensity positively affects the interaction between the boundary layer flow in the vicinity of the wall and the flow in the outer regions.

Ead and Rajaratnam (2002) investigated hydraulic jumps on corrugated beds with three different sinusoidal forms of corrugation, where their relative roughness, t/y_1 , in which t is the corrugation depth and y_1 is the upstream depth, are 0.5, 0.43 and 0.25 respectively. The tailwater depths in jumps on corrugated beds appeared to be appreciably smaller compared to those on smooth beds. Moreover, length of jumps on corrugated beds halved that of the smooth jumps. Further, the integrated shear stress is found to be 10 times of that on smooth beds. The axial velocity profiles along the corrugated bed, on the other hand, were quite similar to those on smooth bed with minor deviations from the simple plane wall jet. The L/y_1 ratio, L being the longitudinal distance where maximum axial velocity, u_m , equals to the half of the upstream velocity, U_1 , was much smaller for the jumps on corrugated beds compared to that of smooth beds. The normalised boundary thickness was 0.45 which surpassed the value of 0.16 for smooth beds indicating that the turbulent mixing through the corrugated channels is approximately threefold the amount of that on the smooth beds.

Negm (2002) collected an extensive amount of data from the empirical work of various experimental studies to develop a design equation for the optimal stilling basin design in hydraulic terms with cubic roughness elements. The equation includes all important flow and roughness parameters such as the supercritical Froude number, the height of the roughness ratio, the length of roughness ratio, the initial length ratio (from the gate) and the roughness density. [See Figure 1.1 and Equations 1.1 and 1.2]

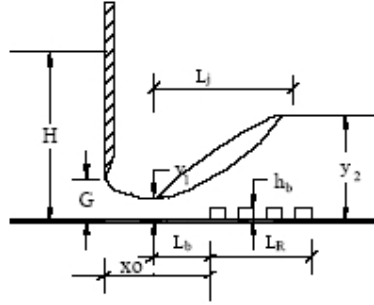


Figure 1.1: Definition sketch for hydraulic jump over roughened bed (Negm, 2002)

$$\frac{y_2}{y_1} = -0.002I + 1.200F_1 - 1.234 \frac{h_b}{y_1} + 0.006 \frac{L_R}{y_1} + 0.009 \frac{x_o}{y_1} + 0.531 \quad [1.1]$$

$$\frac{L_j}{y_1} = 0.112I + 8.228F_1 - 29.874 \frac{h_b}{y_1} + 0.058 \frac{L_R}{y_1} + 0.209 \frac{x_o}{y_1} - 0.597 \quad [1.2]$$

Celik et al. (2003) used prismatic roughness elements to investigate their effect on hydraulic jump properties. They concluded that both the sequent depths ratio and the jump length are negatively affected by the prismatic roughness elements installed into a smooth bed.

Cui et al. (2003) investigated the turbulent flow characteristics of a channel with transverse rib roughness on one wall by Large-Eddy Simulation (LES) technique. The spacing of the roughness elements varied in order to produce d-type and k-type roughness with an additional intermediary roughness between the two. Their research agreed with the prior experimental enquiries in scope of which these rib type roughness classifications have been drawn. Based on their pitch ratios, roughness arrangements are divided into two, namely the d- and k-types. Whereas closely spaced ribs formed d-type roughness where the cavities in-between the elements are filled by a relatively weak eddy that does not interact with the flow outside the roughness layer, the k-type roughness with larger rib spacing generates a main 4 rib-height eddy in the groove between the ribs with several smaller eddies. Since rib spacing larger than 4 rib-heights would capture this larger eddy, 4 is the transitory value for the ratio of rib spacing to rib height

where the transition from d-type to k-type roughness is observed. Furthermore, it is articulated that the ribs on the bottom of the channel influence the resistance on the top wall, which suggests a large scale interaction between the flow in the roughness layer and the outer flow.

Ayanlar (2004) studied the effect of corrugated beds on hydraulic jump properties with altering flow characteristics. Corrugated aluminium sheets of different wavelengths are tested under Froude numbers of 4 to 12. Corrugations are found to reduce the required tailwater depth of the jump for given upstream conditions, y_1 and F_1 , compared to that forming on a smooth bed. An average tailwater reduction factor of 20% and a length reduction factor of 35% are obtained. The gain in energy loss is obtained to decrease with increasing Froude numbers to a minimum value of 7% after a Froude number of 8.

In their study on the turbulence structures of hydraulic jumps of low Froude numbers, Liu et al. (2004) reported that the maximum turbulence intensities with turbulence energies and Reynolds stress decrease rapidly with x/y_2 within the jump and then gradually level off in the transition region from the jump to usual open channel flow, where x is the longitudinal distance of the locus from the channel inlet and y_2 is the subcritical depth.

Bilgin (2005) studied the correlation and distribution of shear stress for turbulent flow in a smooth rectangular basin. Since the structure of the flow in a narrow channel is more complicated as a result of secondary flow formations, Bilgin chose to study on a narrow channel model. He determined that the boundary shear stress approached zero at the corners of the channel and the wetted perimeter. He also reported that in a channel with a certain width-water depth ratio, the flow is three-dimensional as a result of the free surface and secondary flow formation. He proposed a handy equation to designate the dimensionless wall shear stress and boundary shear stress at any section of the channel.

Evcimen (2005) investigated the effects of non-protruding prismatic roughness elements on hydraulic jumps with upstream Froude numbers ranging from 7.3 to 16.6. Roughness elements with four pitch ratios and two different length ratios are tested, where pitch ratio and length ratio are defined as the ratio of the roughness spacing to the roughness height and to the length of a single roughness

element, respectively. In his study, Evcimen concluded that for a given upstream condition, y_1 and F_1 , the tailwater depth in a roughened bed is 20% lower compared to that formed on a smooth bed for a length ratio interval of 4 to 9. The length of jump formed in a roughened bed is obtained to be 40% shorter than that of a smooth jump. Moreover, 5 to 10% higher energy dissipation is observed in jumps forming on rough beds compared to those on smooth beds.

1.3. Aspirations

The fundamental aim of the study is to investigate the effects of the varying upstream flow parameters, i.e. the supercritical Froude number, F_1 , and supercritical depth, y_1 , through with the boundary roughness parameters, as the length ratio, pitch ratio and roughness arrangement, on the hydraulic jump. Energy dissipation rates, variations in jump lengths and sequent depth ratios obtained for different roughness arrangements covered in the study will be assessed in scope of the former work conducted on hydraulic jumps in roughened beds and on smooth channels.

A series of experiments will be carried out on rough beds with different roughness designs which are formed, first, by altering length and pitch ratios, which denote the ratios of roughness spacing to roughness length in the longitudinal axis and to roughness height, respectively, and, secondly, by changing the bed arrangement with staggered roughness elements gone to pieces from strip roughness elements.

The author aims at reaching promising outcomes about non-protruding prismatic roughness strips as reduction in jump length and tailwater depth besides increased energy dissipation compared to jumps on smooth beds. Author's other expectation is to engender the reduction in jump lengths and required tailwater depths besides the increment in energy loss along the bed via generating third-dimensional effects in the turbulent flow section. This is presumed to be realised via breaking the non-protruding strip elements into three equal parts and installing them into the bed in a staggered manner. Moreover, spacing between successive rows of staggered roughness elements will be altered in order to

investigate the effect of different length and pitch ratios on non-protruding roughness elements in staggered arrangement.

1.4. Outline of the Text

In the second chapter of the text (Chapter II), basic characteristics of hydraulic jumps both on smooth and roughened beds will be given in the light of the pertaining literature on the subject. The details of the empirical work as the procedures, channel model, proposed roughness arrangements and measurement equipment will be given in the third chapter (Chapter III). In the fourth chapter (Chapter IV), the results of the experimental runs will be scrutinised and the results obtained will be discussed. In the final chapter (Chapter V), conclusive remarks on the outcomes of the text will be passed.

CHAPTER II

WHAT IS A HYDRAULIC JUMP?

2.1. Fundamentals of Hydraulic Jump

In the following sections, fundamental features of the hydraulic jump will be given in scope of the literature on the hydraulic jump phenomenon. The conjugate depths formulae, energy inequality between the supercritical and subcritical sections, length of jump, water surface profile of the jump, and finally, nature of velocity distribution in the vertical cross-sections through the longitudinal section of the jump are the main headings that will be given in brief through the consequent subchapters.

2.1.1. Conjugate Depths in Classical Jump

An indispensable parameter used in the designation of the flow properties of an unconfined flow is the Froude number, where the average flow velocity at any section of the flow with a known depth is proportioned to the celerity of small disturbances for the same depth of still water. According to Chanson and Montes (1995), Froude number is analogous to the Mach number for compressible flows.

$$F_n = \frac{V_n}{\sqrt{gy_n}} \quad [2.1]$$

where,

F_n is the Froude number at n^{th} section

where,

V_n is the average velocity

g is the acceleration of gravity

y_n is the flow depth

For a typical jump formed on a smooth bed in a rectangular channel as illustrated in Figure 2.1, the conservation of momentum between upstream and downstream sections of the jump and satisfaction of flow continuity leads to the reputed Belanger equation (*Chow, 1959; Rajaratnam, 1967*):

$$\frac{y_2^*}{y_1} = \frac{1}{2} \left(\sqrt{1 + 8F_1^2} - 1 \right) \quad [2.2]$$

where,

y_2^* is the subcritical depth

y_1 is the supercritical depth

F_1 is the Froude number of the supercritical flow

Streeter and Wylie (*1981*) presented a modified form of Belanger equation for a horizontal rectangular channel of constant width by omitting the wall and bed

friction. With the equation, Froude number of the downstream flow can be directly calculated:

$$\frac{F_2}{F_1} = \frac{2^{\frac{3}{2}}}{\left(\sqrt{1+8F_1^2} - 1\right)^{\frac{3}{2}}} \quad [2.3]$$

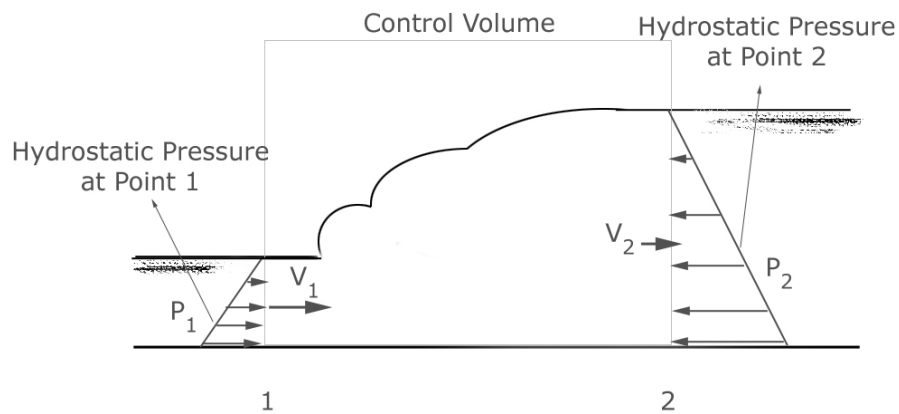


Figure 2.1: A typical hydraulic jump formed on a smooth bed

For the sake of computational simplicity, for relatively large values of supercritical Froude numbers, which is 8 and over for Chow (1959), one can use the following formula rather than Equation 2.2 (Ead and Rajaratnam, 2002):

$$\frac{y_2^*}{y_1} = \sqrt{2} F_1 - 1 \cong \sqrt{2} F_1 = 1.41F_1 \quad [2.4]$$

For flows where $F_1 > 2.5$, Negm (2000) quotes the following approximation given by Hager (1992):

$$Y^* = \sqrt{2} F_1 - \frac{1}{2} \quad [2.5]$$

where,

$$Y^* = y_2^* / y_1$$

Ohtsu and Yasuda (1994), referring to Ohtsu et al. (1990), report that the corrected momentum equation proposed by Rajaratnam (1965) can be used for a better approximation of the sequent depths of Belanger equation:

$$\left(\frac{y_2}{y_1}\right)^3 - \{2F_1^2 + 1 - S_f\} \left(\frac{y_2}{y_1}\right) + 2F_1^2 = 0 \quad [2.6]$$

where,

S_f is the integrated dimensionless bed shear force per unit width in jump:

$$S_f = \int_0^{L_j} 2 \frac{\tau_0}{\gamma y_1^2} dx \quad [2.7]$$

where,

L_j is the length of jump

γ is the unit weight of water

τ_0 is the bed shear stress

Ohtsu and Yasuda (1990) approximated both the data of Rajaratnam (1965) and S_f of Ohtsu et al. (1990) as follows [Figure 2.2]:

$$S_f = 0.12(F_1 - 1)^2; \quad \text{for } 3 \leq F_1 \leq 10 \quad [2.8]$$

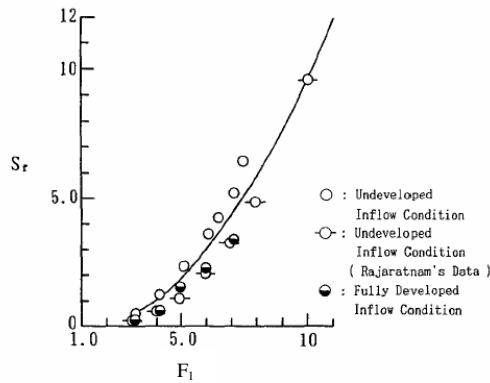


Figure 2.2: Integrated bed shear force as denoted by the solid line (Ohtsu and Yasuda, 1990)

As quoted by Evcimen (2005), Hager and Bremen (1989) report the equation presented by Harleman (1959) to be suitable for the designation of sequent depths ratio:

$$F_1^2 = \frac{1}{2} \frac{Y[(Y+1)(Y-1) + \bar{S}]}{\beta_1 Y - (\beta_2 + J)} \quad [2.9]$$

where,

$$\bar{S} = 2 \frac{F_1^2}{u_1 R_1} \int_0^{L_j} \left(\frac{\partial \bar{u}}{\partial y} \right)_{y=0} dx \quad [2.10]$$

B_i is the momentum correction coefficient at section i , for $i=1, 2$

J is the downstream turbulence-flux correction factor

Y is the sequent depths ratio, $\frac{y_2}{y_1}$

\bar{S} is a non-dimensional bottom shear force

u_1 is the upstream flow velocity

$R_1 = \frac{u_1 y_1}{\nu}$ is the upstream Reynolds number in which ν is the kinematic viscosity of water

2.1.2. Sequent Depths for a Flow under a Sluice Gate

Sluice gate is an upstream control which forms large heads in its upstream. Via the opening at the bottom section of the gate, water is released with high flow velocities [Figure 2.3].

Lin et al. (2002) studied on the distinguishing condition for the flows under sluice gates by the designation of which whether a jump formed at the downstream section of the sluice gate will be free or submerged is determined.

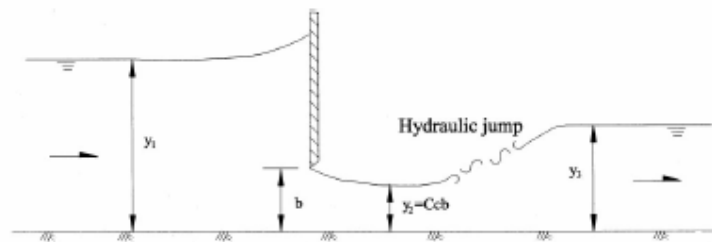


Figure 2.3: Free flow under a typical sluice gate (Lin et al. 2002)

Flow contraction is a common phenomenon for flows under sluice gates. Hence, in the pertaining flow formulae, the effect of sectional contraction should also be taken into account. The degree of the contraction may be represented by a contraction coefficient (*Lin et al., 2002*):

$$C_c = \frac{y_2}{b} \quad [2.11]$$

where,

y_2 is the flow depth at vena contracta, i.e. the shallowest depth in the flow

b is the opening height

The maximum sequent depth can be calculated via substituting the depth at Vena Contracta into y_1 in Belanger equation. Tailwater depths higher than the obtained value will result in a submerged hydraulic jump.

The contraction coefficient was found to be ranging between 0.60 and 0.75 for planar sluice gate depending on the streamline angle with the horizontal (*Montes 1997*).

Lin et al. (2002) found for horizontal streambeds that the contraction coefficient increases from 0.59 to 0.61 with an increase in b/E_1 value, where E_1 is the specific energy at the upstream section.

2.1.3. Energy Dissipation between the Upstream and Downstream Sections

Large amount of energy is dissipated in a hydraulic jump due to eddy and secondary wave formation. Hydraulic jump has been accepted as the most effective and efficient method of dissipating energy for water flowing over a barrage or spillway (*Chaurasia, 2003*). Thanks to the findings of Resch and Leutheusser (1972), now it is a well-known fact that the inflow conditions have considerable effects on the energy dissipation, momentum transfer and air

entrainment characteristics of the hydraulic jump phenomenon (*Chanson and Brattberg, 2000*).

The amount of energy dissipation in a hydraulic jump is designated by the employment of the principles of conservation of energy, momentum and continuity between the upstream and downstream sections of the jump in a horizontal channel. The energy, which is conventionally denoted by E_i at the i^{th} section, is the sum of the depth and velocity head for that given section, measured with respect to the channel bottom:

$$E_1 = y_1 + \frac{q^2}{2gy_1^2} \quad [2.12]$$

$$E_2 = y_2 + \frac{q^2}{2gy_2^2} \quad [2.13]$$

$$E_L = y_1 - y_2 + \frac{q^2}{2g} \left(\frac{y_2^2 - y_1^2}{y_1^2 y_2^2} \right) \quad [2.14]$$

where,

E_L is the loss in energy per unit weight of the flow between sections 1 and 2 [Figure 2.4]

q is the unit discharge

The amount of dissipated energy per unit weight of a fluid flow in a smooth channel can be also expressed as follows (*Chow, 1959*):

$$E_L = \frac{(y_2 - y_1)^3}{4y_1 y_2} \quad [2.15]$$

There is a unique diagram drawn according to the flow and channel-section characteristics which is denoted as the specific energy diagram [Figure 2.4]:

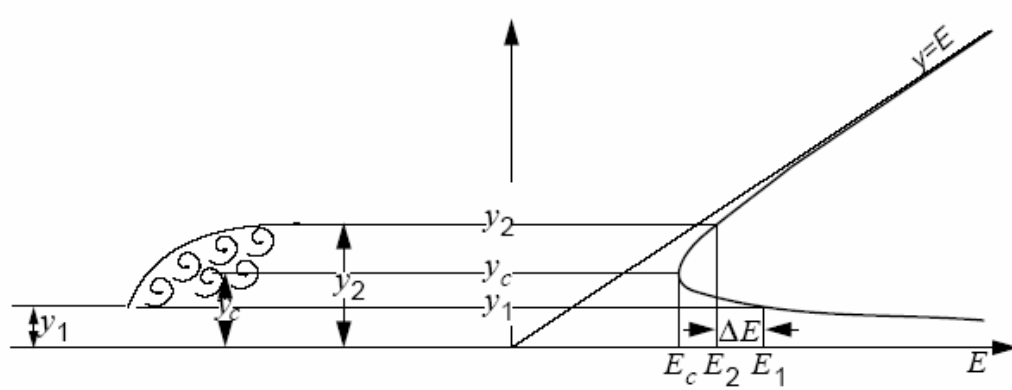


Figure 2.4: Hydraulic jump profile and associated specific energy diagram

Chaurasia (2003) developed equations for the direct conversion of jump and flow parameters on rectangular smooth beds like E_L , y_1 and y_2 and q to one another. Using Equation 2.15, Chaurasia rewrote the energy loss equation as follows:

$$E_L = y_1 \frac{\left[\left(\frac{y_2}{y_1} \right) - 1 \right]^3}{4 \left(\frac{y_2}{y_1} \right)} \quad [2.16]$$

Substituting the conjugate depth ratio (y_2/y_1) in Equation 2.2 into Equation 2.16 led to:

$$E_L = \frac{y_1}{16} \frac{\left(\sqrt{1 + 8F_1^2} - 3 \right)^3}{\left(\sqrt{1 + 8F_1^2} - 1 \right)} \quad [2.17]$$

Substituting the supercritical Froude number into Equation 2.17:

$$E_L = \frac{y_1 \left(\sqrt{1 + 8 \frac{q^2}{gy_1^3}} - 3 \right)^3}{16 \left(\sqrt{1 + 8 \frac{q^2}{gy_1^3}} - 1 \right)} \quad [2.18]$$

In the same way, with the substitution of subcritical Froude number:

$$E_L = \frac{y_2 \left(3 - \sqrt{1 + 8 \frac{q^2}{gy_2^3}} \right)^3}{16 \left(\sqrt{1 + 8 \frac{q^2}{gy_2^3}} - 1 \right)} \quad [2.19]$$

The relative energy loss E_L/E_1 is a dimensionless parameter employed for the designation of the efficiency of the jump. Rajaratnam and Hurtig (2000) give the variation of the relative energy loss with altering supercritical Froude number, as given in Figure 2.5.

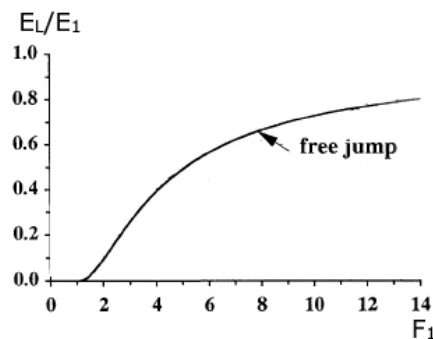


Figure 2.5: Variation of relative energy loss with incoming Froude number
-Modified- (Rajaratnam and Hurtig, 2000)

2.1.4. Length of Jump

The length of the jump, according to which the length of the stilling basin is defined in the design process, is an indispensable feature of the hydraulic jump phenomenon. Hager (1992) lists several features of the state of flow where the longitudinal distance, x_2 , i.e. where the subcritical depth of the jump forms, is presumed to be attained: The flow section where the free surface is essentially level, the surface turbulence has diminished in majority, the deaeration of large bubbles has been completed and/or gradually varied flow conditions reemerge.

With the proper designation of the jump length, the limit where intense turbulence and flow irregularities diminished is determined. Thus, the appropriate locus where the stilling basin will be extended to is determined.

Peterka (1958), regarding Figure 2.6, reported the relative length of the jump for a considerable range of upstream Froude numbers as follows:

$$\lambda_j = 220 \tanh \left[\frac{F_1 - 1}{22} \right], \quad 4 < F_1 < 12 \quad [2.20]$$

or, simply:

$$L_j = 6y_2^* \quad [2.21]$$

where,

$\lambda_j = \frac{L_j}{y_1}$ is the relative length of the jump

L_j is the length of the jump

y_2^* is the sequent depth of y_1 as given in Equation 2.2

Ead and Rajaratnam (2002) developed an equation on the length ratio of both smooth and forced jumps with respect to the inflow condition [See also Fig. 2.6]:

$$\frac{L_s}{y_1} = 2.91F_1 + 5.06 \quad [2.22]$$

$$\frac{L_r}{y_1} = 1.74F_1 + 3.62 \quad [2.23]$$

where,

L_s is the length of jump on a smooth bed

L_r is the length of jump on a rough bed

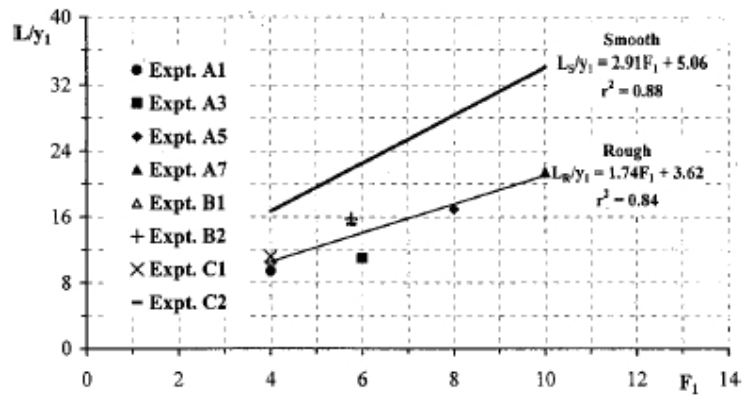


Figure 2.6: Variation of L/y_1 scale with F_1 (Ead and Rajaratnam, 2002)

Again, Negm (2002) proposed a formula where he related length ratio L/y_1 of the classical jump with the upstream Froude number:

$$\frac{L_j}{y_1} = 8.953F_1 - 1.963 \quad [2.24]$$

USBR (1955) reported a chart correlating the length ratio L_j/y_2^* to F_1 , where for $F_1 < 5$ there is a positive correlation, on the other hand, for $F_1 > 5$ the correlation leads to Equation 2.21 as seen in Figure 2.7.

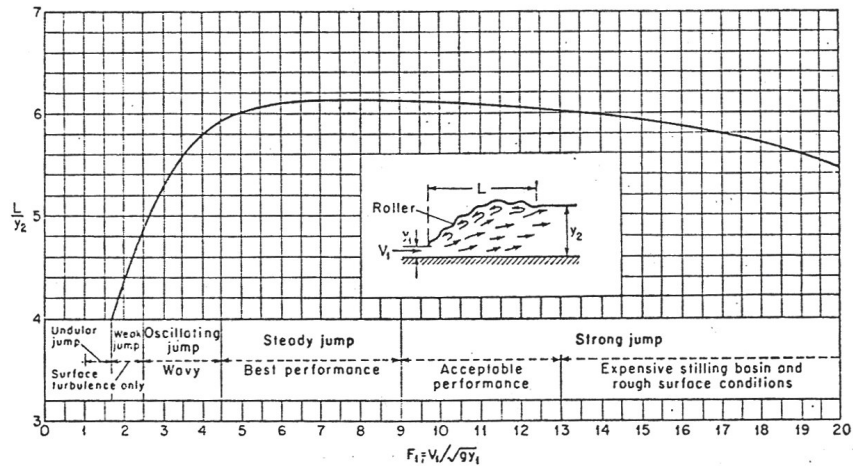


Figure 2.7: Correlation between the subcritical length parameter and F_1 (USBR, 1955)

The empirical determination of the jump length is a non-consensual issue. Hence, a unique assessment process might be necessitated for each unique study. The confusion in jump length determination arises from the various definitions of the depth of the subcritical section.

The beginning or toe of the jump is defined as the initiation point of the abrupt depth change in the flow profile. The sequent depth of the jump, on the other hand, is mostly taken at the section where the variation in depth becomes minimum. However, some investigators take this section where flow profile completely forms and water level becomes constant.

Rajaratnam and Subramanya (1968) compare both approaches in scope of their usage in the empirical work. The approach which proposes to take the section where the mean water surface reaches the maximum depth and becomes level is the popular one. Though, researchers rarely prefer to take the immediate end of

the roller as the sequent depth, given that the flow depth at the end of the roller in level rectangular channels is somewhat less than the subcritical sequent depth. The authors, too, take the length between the toe and the jump end as defined in the first approach. However, this approach leads to large personal errors since the profile changes, where uniform flow conditions form, become so minute that the exact location where subcritical depth forms becomes unidentifiable.

For the present study, the first approach is preferred since in some experiments the downstream profile was not regular due to the locomotion of waves generated by the roller along the downstream sections.

2.1.5. Free Surface Profile and Pressure Distribution

Free surface profile of flowing water refers to the longitudinal mapping of the water depths through the length of the channel where the flow takes place. Water depths, y_n , are plotted with respect to the longitudinal distance taken, x_n , along the channel. For the sakes of simplicity and common consent in profile-building process, the need for an appropriate dimensionless length parameter emerged.

Bakhmeteff and Matzke (1936) used the length parameters $y/(y_2-y_1)$ and $x/(y_2-y_1)$ as the y and x axes where the origin is located at the toe of the jump. Each graph for varying upstream Froude number has given different results as illustrated in Figure 2.8 (Rajaratnam and Subramanya, 1968).

In his study on jumps below drops, Moore (1943) made water depth measurements in the vicinity of the jump toe whereas he directly measured the bed-pressure profile in the remaining larger section in view of the fact that except the initial sections of the jump, bed-pressure values are almost identical with the water depth through the jump.

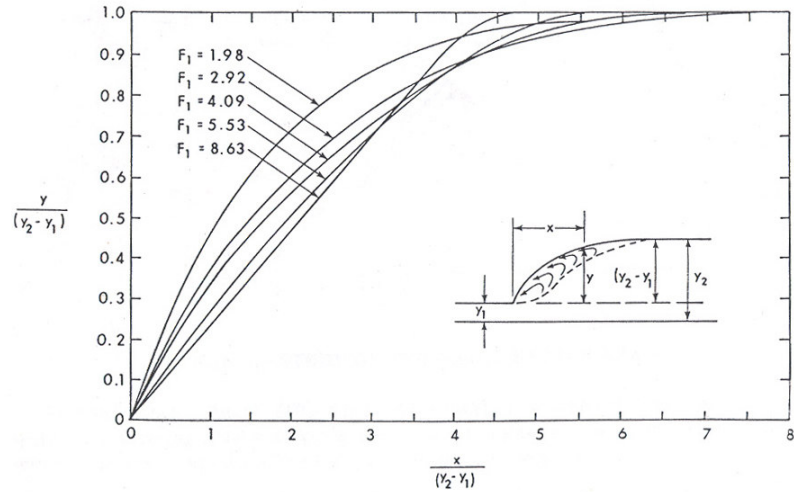


Figure 2.8: Flow profiles of Bakhmeteff and Matzke (1936)

Rajaratnam (1961, 1962), using his measurements on the bed pressure profile, which is essentially identical with the mean water level profile, of a hydraulic jump for incoming Froude numbers of 3.50 to 11.30, presented a correlation among the dimensionless length and depth parameters as shown:

$$\frac{y}{y_2} = A_1 \left(\frac{x}{y_2} \right) + A_2 \left(\frac{x}{y_2} \right)^2, \quad F_1 \geq 5.0 \quad [2.25]$$

where,

A_1 and A_2 are parameters of F_1

Rajaratnam and Subramanya (1968) presented a rather simple method for the bed-pressure and water surface profile prediction on smooth rectangular beds. In scope of this study, data obtained and processed by various researchers have been superimposed on a single profile with the selection of *proper* length parameters as illustrated in Figure 2.9.

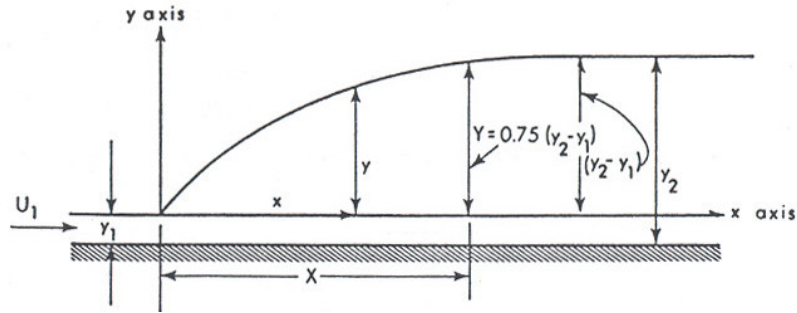


Figure 2.9: Definition sketch of Rajaratnam and Subramanya's (1968) profile

Using the above profile framework and different data from various researchers, Rajaratnam and Subramanya (1968) developed the following relationship where the length scale X is related to the supercritical Froude number and depth:

$$\frac{X}{y_1} = 5.08F_1 - 7.82 \quad [2.26]$$

2.1.6. Velocity Distribution along the Jump

Hager and Bremen (1989) investigated the velocity profiles of a smooth jump with respect to the length scale X , where X is the ratio of the longitudinal distance along the channel to the roller length. They plotted the schema presented in Figure 2.10.

The reverse flow begins at the section where the toe of jump is located and extends through the end of the roller. However, through the final sections of the jump length, the velocity profile seems to have already begun to transform into a uniform flow. The dotted line represents the turnover point of the velocity vector. On the other hand, in the section separated by the dashed line, the domain where roller governs is illustrated.

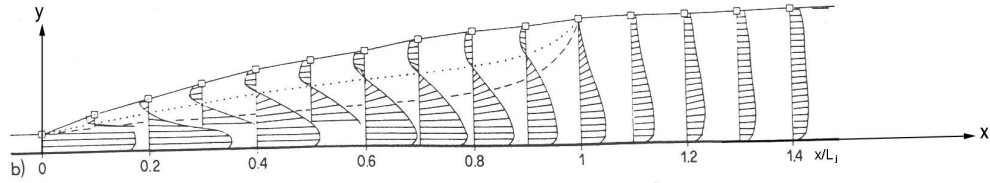


Figure 2.10: Velocity profiles in classical hydraulic jump for $F_1=4.30$ (Hager and Bremen, 1989)

In the section remaining below the dotted curve, there is a narrow section where the depth derivative of the vertical velocity function is positive, i.e. $\partial u/\partial y > 0$. It is commonly termed as the boundary layer portion above which a free-mixing or diffusion portion rests with a negatively sloped velocity profile. In the reverse flow slice located above the dotted curve, velocity vectors are reversed and the depth derivative of the velocity function is negative, or namely $\partial u/\partial y < 0$ [Figure 2.11].

In this sketch, u_m is the maximum cross-sectional velocity and δ_1 is the flow depth where cross-sectional velocity equals $u_m/2$ with a negative slope and δ is the height of the boundary layer. Rajaratnam (1965) developed a correlation between the velocity and depth parameters in the share where the slope of the profile is positive as shown in Equation 2.27 (Hager, 1992):

$$\frac{u}{u_m} = 2 \left(Z_\delta 10^{1-Z_\delta} \right)^{0.12}, \quad 8.3 < \frac{x}{y_1} < 41.7 \quad \text{and} \quad 3.9 < F_1 < 9.05 \quad [2.26]$$

where,

$$Z_\delta = \frac{5y}{\delta_1}$$

Though the maximum velocity forms at $y/\delta_1=0.2$ according to Equation 2.26, Rajaratnam (1965) calculated that length approximately as 0.18 (Hager, 1992).

Regarding the parameter, δ_1 , experimental results can be given via the following equation:

$$\frac{\delta_1}{y_1} = 1 + \frac{1}{15} \left(\frac{x}{y_1} \right), \quad \frac{x}{y_1} < 30 \quad [2.27]$$

Keeping in mind that Rajaratnam's data fail to include the section where the roller reigns, the streamwise decay of the maximum velocity can be approximated by the formula given in Equation 2.28:

$$\frac{u_m}{u_1} = \frac{1}{42} \left(45 - \frac{x}{y_1} \right), \quad \frac{x}{y_1} < 30 \quad [2.28]$$

For $x/y_1 > 30$, the function given in Equation 2.28 converges to zero.

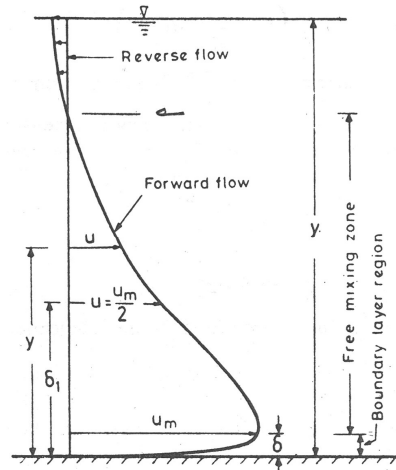


Figure 2.11: Velocity profile at a single section (Rajaratnam, 1965)

2.2. Jump Taxonomy regarding the Supercritical Condition and Surface Profile

Thanks to extensive studies of Bradley and Peterka (1957), hydraulic jumps are classified under five headings with respect to the Froude number of the supercritical section in horizontal rectangular channels.

Undular jumps [Figure 2.12] form when the Froude number of the inflow is extremely close to the critical value, 1. For Froude numbers below 1.7, an undulating jump forms when the momentum of the upstream section equals the downstream value. Undulations on the water surface form with an extremely small ripple on the surface. The sequent depth ratio is close to 1 and the energy loss per unit specific energy of the upstream section is practically zero.

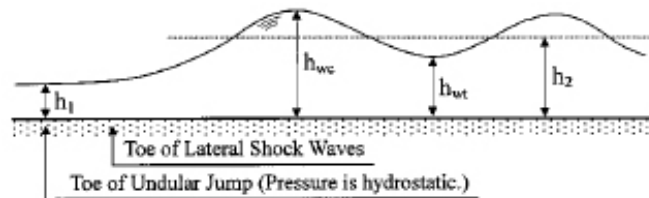


Figure 2.12: An undular jump profile (Ohtsu et al., 2003)

The surface roller commences to become visible after supercritical Froude number exceeds 1.7 through 2.5. In this interval, the jump is weak and the roller still lacks maturity. The energy loss is around 5% at $F_1=1.7$, and 18% at $F_1=2.5$. The water surface is smooth after the jump section.

Usually an oscillating jump forms when $2.5 < F_1 < 4.5$. The incoming high-velocity flow oscillates between the bed and free surface chaotically which results in instability of jump. Large surface waves are generated as a result of the oscillations which travel considerable distances downstream. Energy dissipation is moderate with 45% (E_L/E_1) around a supercritical Froude number of 4.5.

Between the supercritical Froude numbers of 4.5 and 9, a well-established jump forms with a fully-developed roller and jump action. An appreciable amount of energy loss is attained. The relative energy loss, E_L/E_1 , ranges from 45% at the

lower and 70% at the upper boundary of the given interval of Froude numbers. Called “steady”, the jump formed in this range of Froude numbers is among the most sensitive in terms of the toe position compared with other types. A minor change in the tailwater depth alters the longitudinal position of the toe significantly.

For supercritical Froude numbers greater than 9, a strong or choppy jump forms. As its name indicates, the water surface is very rough and choppy along the jump. High amplitude waves, which are generated by the jump body, travel at the downstream sections of the jump. The sequent depth ratio is considerably high with intense energy dissipation rates exceeding 70%.

It should be kept in mind that the taxonomy given above has been constructed on purely subjective grounds based on the observation of gross physical similarities among jumps within each type. Henceforth, the given intervals must not be taken as rules of thumb. The effect of local factors might gain superiority over the flow parameter (*Subramanya, 1986*).

2.3. Definitions and Parameters Employed in the Present Study

The length parameters that will be used in this study are given in Figures 2.13, 2.14 and 2.15:

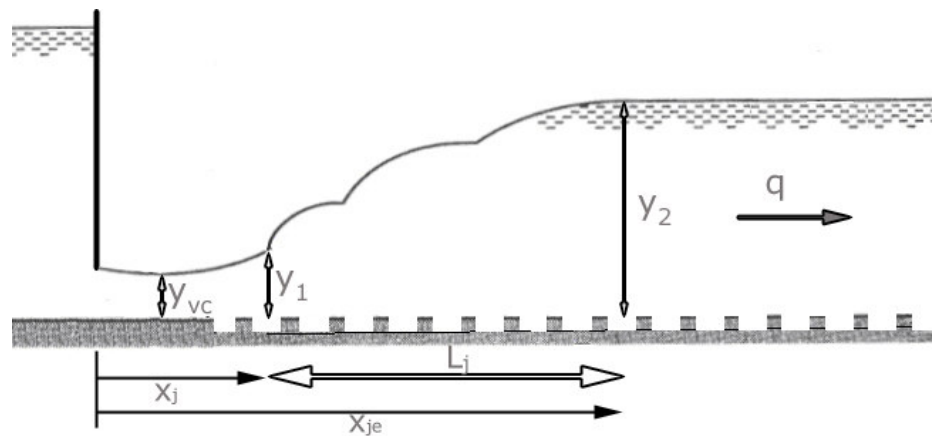


Figure 2.13: Length parameters of the recent study [1]

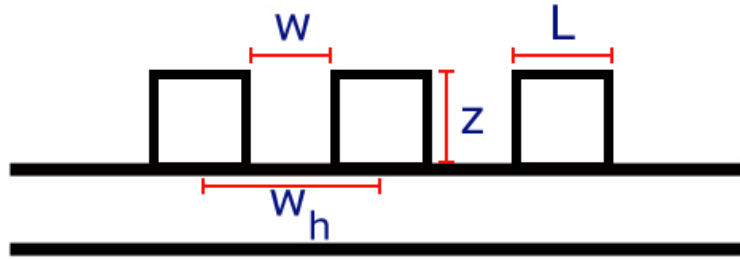


Figure 2.14: Length parameters of the recent study [II]

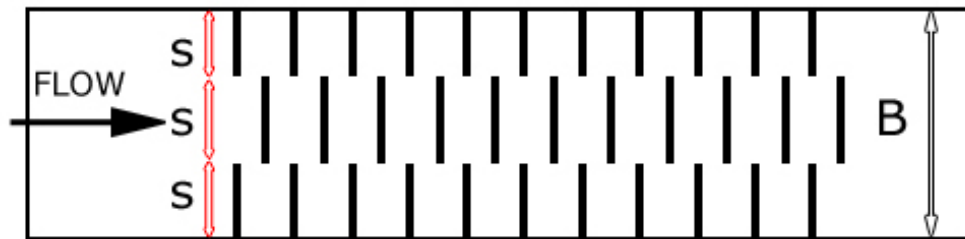


Figure 2.15: Length parameters of the recent study [III]

The tailwater depth, y_2 , and the length of the jump, L_j , can be written as a function of the following parameters:

$$y_2 = f_1(y_1, s, L, z, w \text{ or } w_h, B, q, g, \rho, \mu) \quad [2.29]$$

$$L_j = f_2(y_1, s, L, z, w \text{ or } w_h, B, q, g, \rho, \mu) \quad [2.30]$$

where,

y_2 is the subcritical flow depth from the crests of the roughness elements

L_j is the length of jump

y_1 is the supercritical flow depth from the crests of the roughness elements

s is the width of the roughness elements

B is the channel width

L is the length of the roughness element

z is the height of roughness element

w is the longitudinal spacing between two roughness elements in successive rows from the internal edges

w_h is the longitudinal spacing between two roughness elements in successive rows from the centres

q is the unit discharge

g is the global acceleration of gravity

ρ is the mass density of water

μ is the dynamic viscosity of water

If y₁, q and ρ are selected as repeating variables, the following dimensionless parameters may be found:

$$\frac{y_2}{y_1} = f_3 \left(\frac{q^2}{gy_1^3}, \frac{s}{y_1}, \frac{L}{y_1}, \frac{z}{y_1}, \frac{w}{y_1} \text{ or } \frac{w_h}{y_1}, \frac{\rho q}{\mu} \right) \quad [2.31]$$

$$\frac{L_j}{y_1} = f_4 \left(\frac{q^2}{gy_1^3}, \frac{s}{y_1}, \frac{L}{y_1}, \frac{z}{y_1}, \frac{w}{y_1} \text{ or } \frac{w_h}{y_1}, \frac{\rho q}{\mu} \right) \quad [2.32]$$

To compare the classical hydraulic jump with those formed in rough beds, the length parameter y₁ will be replaced by the conjugate depth of supercritical depth, y₂^{*}, corresponding to the conjugate depth of a classical hydraulic jump

formed on a smooth bed (*Ead and Rajaratnam, 2002*). Since viscous forces may be assumed as insignificant compared to the gravitational force, Reynolds number, $\frac{\rho q}{\mu}$, will be omitted (*Rajaratnam, 1965*).

The first parameter is the square of supercritical Froude number, F_1 . The third, fourth and fifth length parameters can be combined in the pitch ratio, w/z or w_h/z , and the length ratio, w/L or w_h/L . For staggered roughness, the ratio of roughness width to the width of channel, s/B , is a relevant parameter. Therefore, Equations 2.31 and 2.32 can be rearranged as:

$$\frac{y_2}{y_1} = f_3 \left(F_1, \frac{w}{L} \text{ or } \frac{w_h}{L}, \frac{w}{z} \text{ or } \frac{w_h}{z}, \frac{s}{B} \right) \quad [2.33]$$

$$\frac{L_j}{y_2^*} = f_4 \left(F_1, \frac{w}{L} \text{ or } \frac{w_h}{L}, \frac{w}{z} \text{ or } \frac{w_h}{z}, \frac{s}{B} \right) \quad [2.34]$$

CHAPTER III

EXPERIMENTAL SETUP AND PROCEDURES

3.1. Description of the Experimental Setup

The flume where hydraulic jumps have been produced was 0.253 m in width, 0.423 m in depth and 7.35 m in length with Perspex sides in the measurement locus which is 3.67 m in length and concrete sides in the remaining sections. Roughness elements were placed in the first 3.50 m of the Perspex section of the channel and all measurements have been taken in between this range. Tailwater depth was controlled by an adjustable tailgate located at the end of the flume. Experimental setup is illustrated in Figure 3.1.

In the flume, a pressure tank provided the inflow conditions such as the discharge, supercritical depth and Froude number. Schematic representation of the pressure tank with a profile view is given in Figures 3.2 and 3.3.

Water has been supplied to the pressure tank by a constant head tank in the Hydromechanics Laboratory at METU. The discharge was adjusted for each run by the regulating valve installed to the feeding pipe. Water has been collected in a regulating basin following the free fall formed by the tailgate which, again, was connected to a return channel 0.25 m in width, 0.40 m in depth and 9 m in length. Discharge measurements have been made by a V-notch with a 30° notch angle. The point gauge used to measure the water depth on the weir was installed at the end of the return channel. Pressure tank is designed such that the bed of the tank outlet is 3 cm higher than the channel bed elevation which provided us the opportunity to coincide the crests of the roughness elements on the same elevation with the tank outlet base.

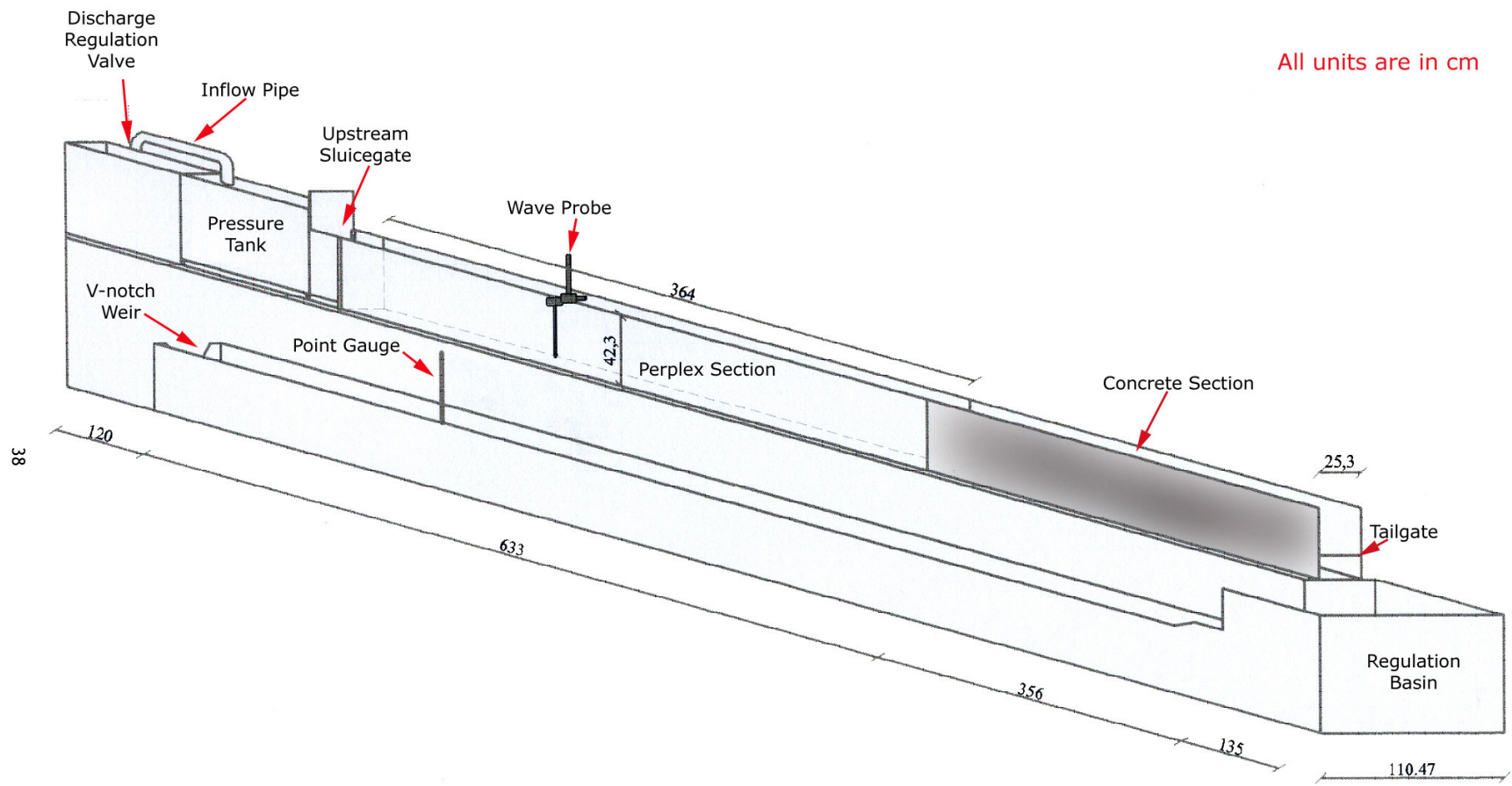


Figure 3.1: Schematic Representation of the Experimental Setup -
-Modified-(Evcimen, 2005)

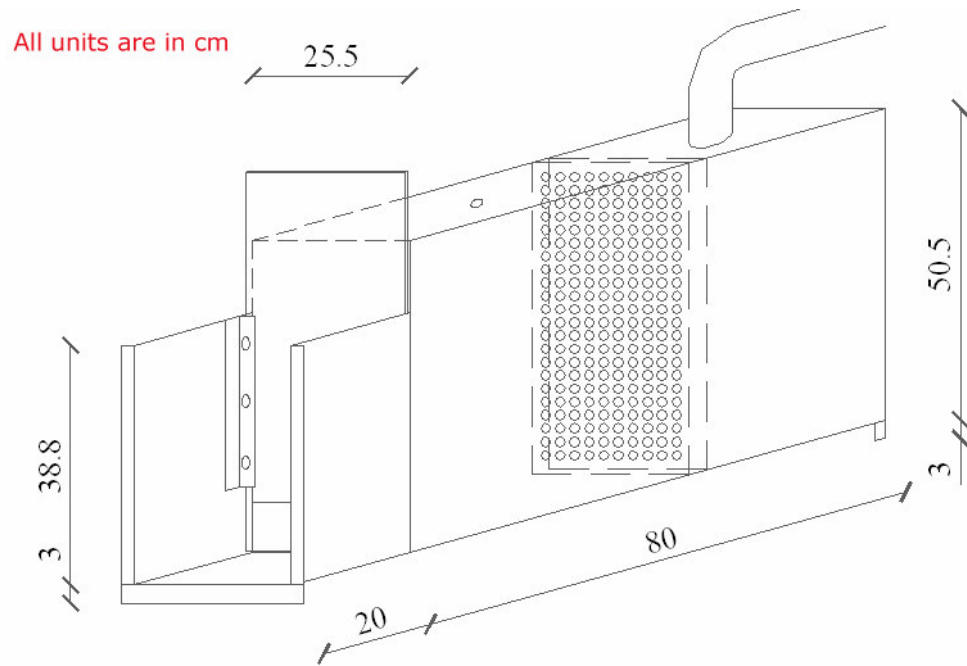


Figure 3.2: Dimensioning of the pressure tank (Evcimen, 2005)



Figure 3.3: General view of the pressure tank

3.2. Features of the Roughness Elements Used

Basically two types of roughness arrangement were used in this study. One is the strip arrangement in which roughness elements extend the whole channel width, and the other is the staggered arrangement which is illustrated in Figure 2.15. Staggered roughness elements are produced by piecing strip roughness bars into three equal parts in width.

Roughness elements in strip arrangement are 1.5 cm in length (L), 1 cm in height (Z) and 25.3 cm in width, which is, indeed, the channel width. The longitudinal spacing between the centres of successive strip or staggered roughness elements, w_h , is the fundamental variable of the experiments. This variable is set to 4.5, 6, 7.5, 9, 10.5, 12, 13.5, and 18 cm for roughness elements both in strip and staggered arrangement. The lateral spacing parameter, s , is kept constant at 8.4 cm which is one third of B . Investigating the effects of lateral spacing, s , on hydraulic jumps formed on artificially roughened beds is a concern of further scrutiny and labour which exceeds the limits of the present study. Practicality of roughness production was the chief concern for assigning this alternative as the representative staggered roughness arrangement.

Since the height of the fiberglass roughness elements is 1 cm, the height of the embedded fiberglass plates is adjusted to 2 cm to satisfy the “no protrusion into flow” criterion of the roughness elements. Roughness elements are screwed into the holes drilled in the embedded plates in regard to preliminary calculations and taking the uncovered arrangements in the previous works into account.

3.3. Calibration of the V-notch Weir

The V-notch weir attached to the end of the return channel has been calibrated by Evcimen (2005). He obtained the three-dimensional velocity profiles at different sections of a flow run via 4 Pitot static tubes in order to calculate the discharge of the flow with the continuity equation [Equation 3.1]. He also measured the water head over the V-notch weir via a point gauge located at 1 or 2 m upstream the weir.

$$Q = \sum_{i=1}^N \Delta Q_i = \sum_{i=1}^N u_i y_i b \quad [3.1]$$

where,

ΔQ_i is the volumetric discharge for each crosssection with an area of ΔA_i

u_i is the crosssectional average velocity of ΔA_i , obtained by numerical integration at i^{th} section

y_i is the depth of flow at i^{th} section

N is the number of sections

When he plotted his depth measurements with the well-known discharge equation [Equation 3.2] for the V-notch weir, the contraction coefficient, C_c , of the V-notch is obtained.

$$Q = \frac{8}{15} C_c \tan \frac{\alpha}{2} \sqrt{2g} H^{\frac{5}{2}} \quad [3.2]$$

where,

α is the notch angle which is 30 degrees for our case

H is the head measured above the V-notch

The contraction coefficient is reported as 0.58 for the V-notch in question (Evcimen, 2005).

3.4. Experimental Apparatus

A point gauge, a wave probe, an HR Wallingford Lab-card (Wave Probe Monitor) hardware and software adjusted to make measurements in ± 5 volt interval, an analogue to digital signal converter and a PC under DOS operating system have been used at the experimental stage of the study [Figure 3.4].

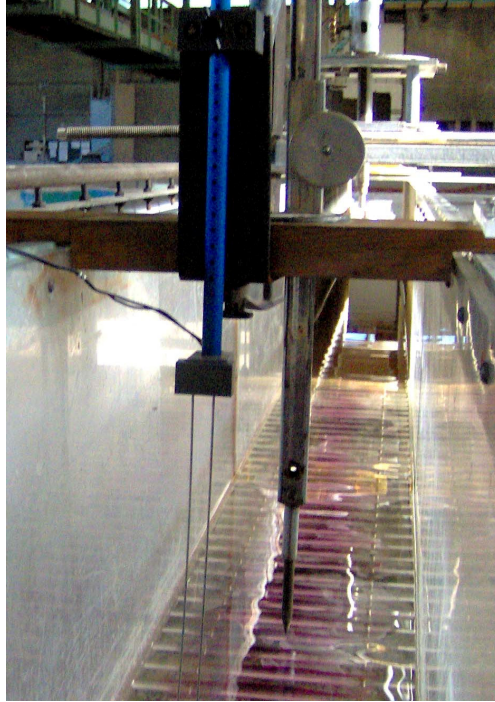


Figure 3.4: Wave probe and point gauge

3.5. Experimental Procedures

In the experiments, following measurements have been made:

- I. In some days, several runs have been performed. Before the first run of each day, the calibration of the wave probe is performed. The stilling basin is filled with water and the depth of the water is kept constant via the tailgate in each step of the calibration process. After each filling and depth adjustment process, a

certain time is spent on stilling the water. Measurement at each successive stage has been conducted once the waves travelling through the basin diminished. When the stillness of the water in the basin is satisfied, depth of the water is measured via the point gauge. Afterwards, wave probe is placed at the same locus and 10 samples, which are the voltage readings stored in the computer, are taken. For each successive stage, the water level is reduced by releasing water from the tailgate. After the tailgate is shut, another run is performed when the stillness of the water is provided. After 10 runs in total, data obtained both from the wave probe and point gauge are processed in an Excel sheet and a voltage versus depth equation is obtained.

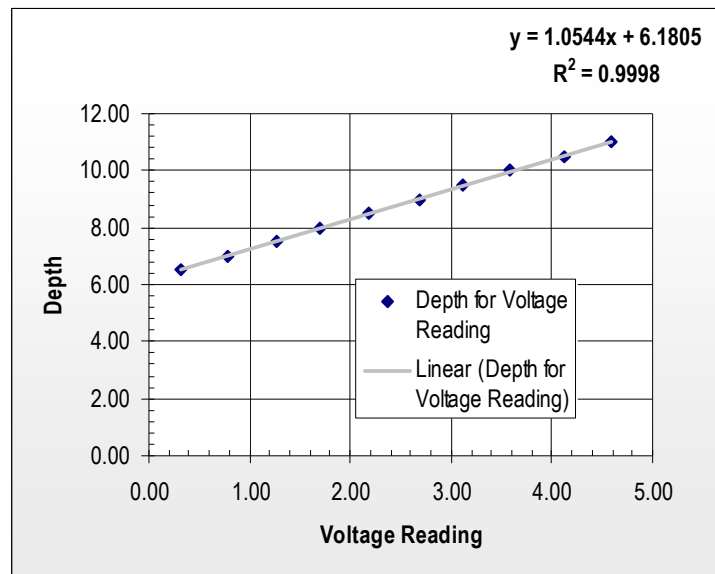


Figure 3.5: Wave probe calibration formula obtained in one of the runs

II. After the calibration data is obtained, discharge regulating valve was opened and in order to form the hydraulic jump at the desired location, tailgate was adjusted. After the formation of the mature flow profile, depth at successive loci has been measured by shifting the wave probe 5 cm downstream through the longitudinal axis of the flume after each measurement. The origin of the x-axis is assigned to be the intersection line of the pressure tank bed and the crest of the initial roughness element which is screwed to the uppermost edge of the

embedded fiberglass plate. At each measurement locus, 100 samples with 0.1 Hz input ratio have been taken via the software installed to the computer. Since the flow surface was rough and wavy at many sections of the jump body, 10 samples would be inappropriate [Figure 3.6]. The average of these 100 samples gave the time-average of the depth at each measurement point. Measurement was truncated each time the downstream depth had become level. Data, stored in “.dat” format, are processed in Excel. The average depth measured for each measurement point is plotted against the longitudinal distance for each run and the surface profile is sketched.

III. In most of the runs, another profile is drawn by making depth measurements with the point gauge at same loci with the wave probe.

IV. The sequent depths, y_1 and y_2 , of the jump were measured by the point gauge.

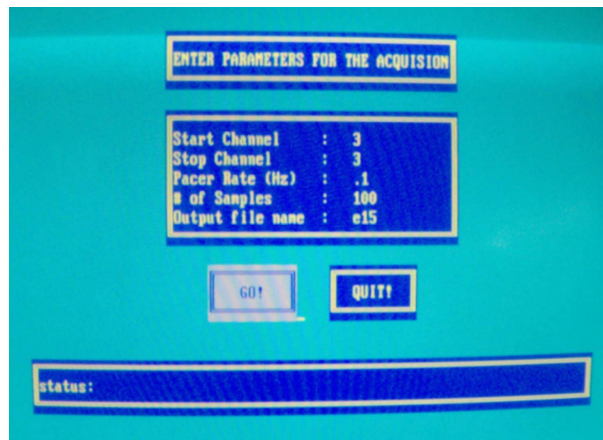


Figure 3.6: A screenshot of the Labcard software

V. Distances where the toe of the jump, x_j , and subcritical depth, x_{je} , formed were measured by the apparatus employed for probe-shifting. The end of the jump was assigned as the initial point where approximately equal flow depths immediately after the jump had been measured successively.

VI. The head value on V-notch was measured 1 or 2 m upstream the notch in order to avoid the depth reduction observed at the notch due to the disturbance in the uniformity of flow at the notch section.

VI. High-resolution photographs of each profile were taken in order to record the flow characteristics in the flume. Grids drawn on the Perplex walls facilitated measurements via high-resolution photography.

The Froude number ranges obtained in the experimental runs performed are $3.64 < F_0 < 14.21$ for Vena Contracta and $2.13 < F_1 < 11.92$ for the toe section. The range of length ratio, on the other hand, is $2 < w/L < 11$. The interval of tested pitch ratios is $3 < w/z < 16.5$.

CHAPTER IV

DISCUSSION OF RESULTS

4.1. Overall Assessment of Experimental Runs

Among 110 in total, 92 experiments have been processed in scope of the study. The ones excluded were those led to improper results due to excessive bucket formation through the flume, where bucket formation stands for the oblique trajectory of flow along the channel. 28 out of 92 experiments tested beds with staggered roughness elements. Most of the experiments carried on to test staggered roughness arrangement could not be conducted since high F_1 values and length and pitch ratios resulted in bucket formation rather than a mature hydraulic jump.

Tests on smooth jumps have not been carried out given that data obtained from Evcimen's study (2005) and USBR (1955) provided the author with necessary data on smooth beds. In the comparison of data on jumps hitherto obtained, tests conducted both on smooth and roughened beds in the literature were taken into consideration.

In the experiments, the w/L ratios (length ratio hereafter) 2, 3, 4, 5, 6, 7, 8 and 11 with w/z ratios (pitch ratio hereafter) 3, 4.5, 6, 7.5, 10.5, 12, 16.5 for both strip and staggered roughness arrangements have been tested. However, only strip roughness arrangements with length ratios 2, 3, 4, 5 and 6 and staggered roughness arrangements with length ratios 2, 3 and 4 have resulted in processable data since bucket formation and instability in jump structure led to corrupt data which resulted in exclusion of regarding experiments.

Throughout the experiments, researcher encountered jump types classified in Section 2.2. In some instances, undular and weak jumps observed at upstream Froude numbers exceeding 2 and 2.5, respectively, which is most probably the outcome of roughness elements installed at the bed level. As the longitudinal spacing between roughness elements increase, intrusion of roughness elements into flow or intrusion of streamlines in between the roughness elements becomes a common phenomenon for flows with low incoming Froude numbers.

The supercritical Froude number, F_1 , of the jump illustrated in Figures 4.1 and 4.2 is 9.65. Hence, it can be classified as a choppy jump. In Figure 4.2, it is observed that the jump switches between the forms shown in Figures 4.1 and 4.2. As seen in the latter case, waves generated by the roller tend to move downstream the channel.



Figure 4.1: A view of steady jump ($F_1=9.65$) [I]



Figure 4.2: A view of choppy jump ($F_1=9.65$) [II]

Hence, making water depth measurements via a wave probe and thus capturing all depth values realised in a time interval are indispensable concerns in a phenomenon like hydraulic jump, where intense variation in parameters observed.



Figure 4.3: Weak jump formation

In Figure 4.3, a weak jump formed on a strip roughness arrangement with a length ratio of 8 is illustrated. The Froude number at Vena Contracta, F_0 , is 3.85. However, since successive roughness elements are located centrally 13.5 cm away from each other, water-depth measurement is prone to fail. When there is large spacing between roughness elements, flow may dive into the channel bottom between the roughness elements. This may cause the surface of flow to be wavy, as illustrated in the figure above.



Figure 4.4: A view of jump for strip roughness with $w/L=4$, $w/Z=6$, $F_0=5.08$, $F_1=3.28$

Another factor triggering wavy downstream profile is the unregulated tailwater, such that the jump formed at the immediate downstream of the sluice gate, the waves on the tailwater-depth-section diminish as shown in Figure 4.5.



Figure 4.5: A view of jump over a strip roughness of $w/L=4$, $w/Z=6$, $F_0=5.08$, $F_1=4.02$

The roughness type and arrangement of the beds shown in Figures 4.4 and 4.5 are the same. Besides, flow parameters except F_1 are practically identical. In the second run shown in Figure 4.5, the location of the jump is shifted upstream towards the sluice gate with the adjustment of the tailwater depth. Consequently, the flow profile of this case is smoother compared to the former case, presented in Figure 4.4. In regard to the taxonomy presented in Section 2.2, the jump shown in Figure 4.4 falls into the oscillating jump category. Waves traveling downstream support this stance. Still falling into the oscillating jump category, the jump shown in Figure 4.5 is more stable.



Figure 4.6: Steady jump [Reflection of the flasher is dimmed]

The jump illustrated in the former case forms with a lower Froude number which is most probably the outcome of the dissipation of certain amount of energy between Vena Contracta and toe of the jump.

In Figure 4.6, an example for a steady jump is illustrated. The supercritical Froude number, F_1 , of the jump is 7.29 which is in between 4.5 and 9.

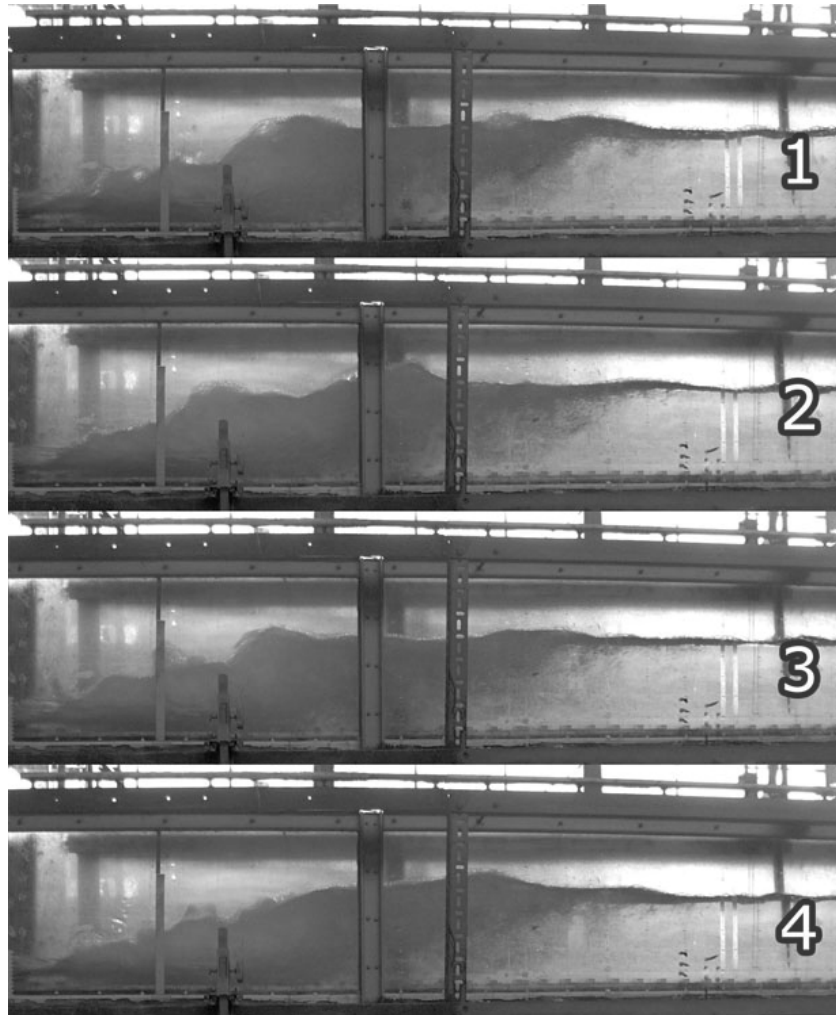


Figure 4.7: Burst shooting of a choppy jump

In Figure 4.7, burst shootings of a choppy or strong jump are given. The turbulence induced in the roller is tremendous. Large waves extend downstream the channel. Air entrainment at the toe is excessive and air bubbles travel a considerable distance downstream. Designation of the location of the sequent

depth, x_{je} , is quite challenging due to the large-amplitude waves generated. Besides its practicality, time-averaged depth measurement via a wave probe is an absolute necessity in such cases.

For length ratios over 7 and F_0 values greater than 3.08, it is observed that flow dynamics are governed by the bucket effect in strip roughness arrangements [Figure 4.8]. Evcimen (2005) had reported this value as 14 on account of the coverage of his study. For staggered roughness arrangements, this value reduces to 4. Indeed, staggered roughness arrangements are quite vulnerable to bucket formation since staggered arrangement results in larger longitudinal spacing between two successive rows in the same column.



Figure 4.8: Bucket effect

Two methods to avoid this handicap might be densification of the roughness elements located at the flume inlet while leaving others untouched and adjusting the tailwater depth in order to form the jump immediately downstream the sluice gate. In this study, the second approach is adopted both to obtain uniform data sets for all sets of experiments and to investigate the variations in jump characteristics with different jump locations.

In the experiments carried out in order to test the effects of staggered roughness on hydraulic jump formation, some additional observations have been made. For instance, separation leading to bucket formation is very common in flows with high incoming Froude numbers. The primary reason for this tendency might be the increased instability in the flow due to pieced structure of the roughness elements. Even though the conventional definition of the length ratio has been

employed for staggered roughness arrangements, a ratio defining the distance between successive single or double rows may be more appropriate. As illustrated in Figure 4.9, twice the space between two successive roughness rows, $2w_h$, may be a better defining factor in determination of jump characteristics.

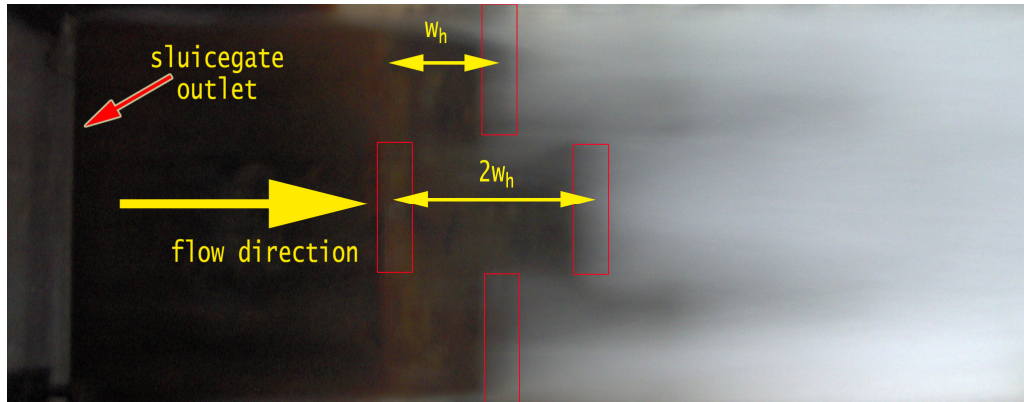


Figure 4.9: Bucket effect initiation at 2nd and 3rd rows

For lower incoming Froude numbers, bucket effect initiates closer to the sluiceway outlet. For F_1 values exceeding 8, bucket effect shifts downstream as illustrated in Figure 4.10.

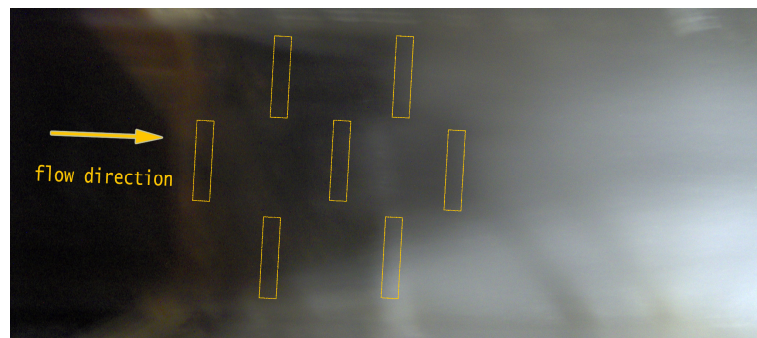


Figure 4.10: Separation observed at 4th and 5th rows

In some of the cases, a stable jump at the immediate downstream of the sluiceway gate could be formed by regulating the flow via tailwater gate. In these cases,

experiments have been successfully carried out. Experiments where the jump was erratic in nature, however, could not be conducted since jumps usually evolved into bucket flow immediately.

In staggered roughness experiments, a boiling-like surface is observed throughout the roller which was not the case for strip roughness experiments. Flow surface was quite irregular along the channel.

4.2. Energy Dissipation at the Jump Upstream

As aforementioned, Vena Contracta is the smallest flow section, thus, the location where the lowest depth is observed in a flow. Vena Contracta forms in flows under sluice gates which do not possess streamlined lip [Figure 2.13].

Chow (1959) reported the depth at Vena Contracta as:

$$y_{vc}=0.61a \quad [4.1]$$

where,

y_{vc} is the flow depth at Vena Contracta

Rajaratnam (1977) found the longitudinal distance where Vena Contracta forms as:

$$x_{vc}=2a \quad [4.2]$$

where,

x_{vc} is the longitudinal distance from the gate to Vena Contracta

Some researchers use sluice gates with streamlined lips in order to obtain an initial water depth that equals the gate opening, a [Figure 4.11A].

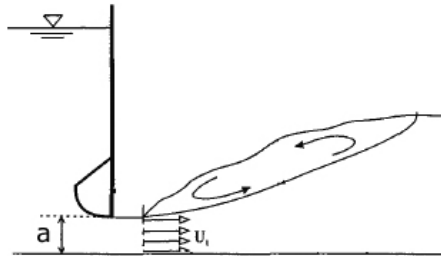


Figure 4.11A: Sluice gate with a streamlined lip

The relative energy loss, $\Delta E/E_{vc}$, is the ratio of energy dissipated between the Vena Contracta and toe of the jump to the energy at the Vena Contracta. This relative energy loss may become important for artificially roughened beds. Let $\Delta x/y_{vc}$ denote the relative distance between the Vena Contracta and the toe of the jump as shown in Figure 4.11B. The relative energy loss, $\Delta E/E_{vc}$, versus $\Delta x/y_{vc}$ is plotted in Figure 4.12 both for artificially roughened beds and smooth beds.

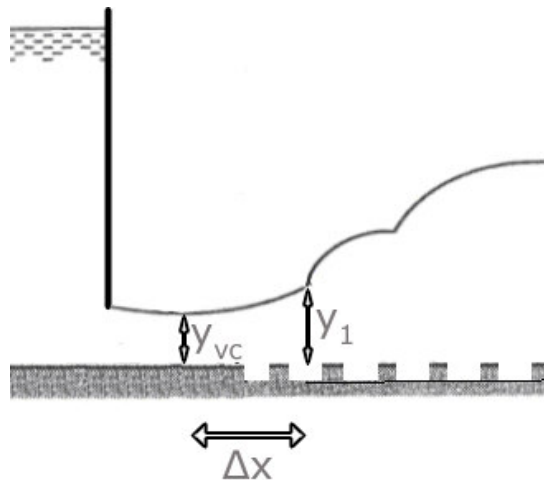


Figure 4.11B: Length parameters of pre-jump energy loss

Figure 4.12 shows that less energy is dissipated prior to jumps formed closer to the sluice gate compared to those formed downstream the channel. Conversely, if the jump locations shifts from sluice gate to the downstream of channel, more energy is dissipated prior to the jump toe.

Furthermore, when the pre-jump energy loss rates for roughened beds and smooth beds are compared, it is seen that while pre-jump energy loss rate on smooth beds is constant around 10%, it increases with higher $\Delta x/y_{vc}$ values for rough beds.

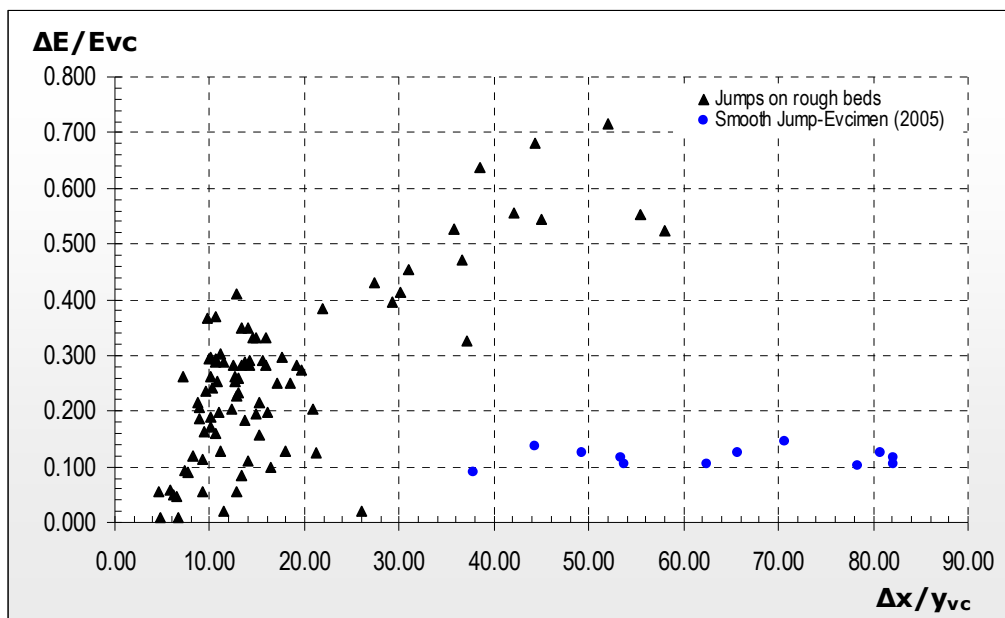


Figure 4.12: Relative energy loss in the channel prior to jump for rough and smooth beds

Regarding Figure 4.12, as jumps get farther through the channel, more energy is dissipated at the upstream sections of the jump. The intense turbulence and eddy formation observed in the cavities between the roughness elements before the toe of the jump might be the main reason of this tendency.

4.3. Energy Dissipation along the Channel

Energy dissipation ratio, $\Delta E/E_1$, is the ratio of the difference between the specific energies of the supercritical and subcritical sections of the jump to the specific energy of the supercritical section. The amount of energy lost along the jump while the flow passes from supercritical state to subcritical state is denoted by the energy loss parameter, ΔE .

Energy dissipation rates for different length and pitch ratios are plotted with regard to the incoming Froude numbers for strip roughness and staggered roughness in Figures 4.13 and 4.14 respectively.

As seen in Figure 4.13, length ratio has no significant effect on the rate of energy dissipation along the jump for strip roughness elements. Similarity with Evcimien's experiments for a length ratio of 4 can be seen in the figure. In Figure 4.14, the effect of incoming Froude number on energy dissipation rate is presented with respect to varying length ratios for staggered roughness elements. Again, Figure 4.14 shows that energy dissipation is basically a function of upstream Froude number, F_1 , and does not depend on length ratio, w/L , and pitch ratio, w/Z .

Figures 4.13 and 4.14 show that the energy dissipation rate for both strip and staggered roughness reaches asymptotic values of 0.8 and 0.75, respectively as F_1 increases.

The relative energy dissipation for strip, staggered roughness and for corrugated beds are shown in Figure 4.15. Figure 4.15 shows that staggered roughness elements dissipate insignificantly higher values of specific energy compared to strip roughness elements. Furthermore, Figure 4.15 shows that corrugated beds are more efficient than prismatic roughness elements for Froude numbers lower than 8.

The discrepancy observed between the recent and previous works in Figure 4.15 might be the outcome of experimental errors and/or variations in definitions of certain parameters as the bed surface elevation.

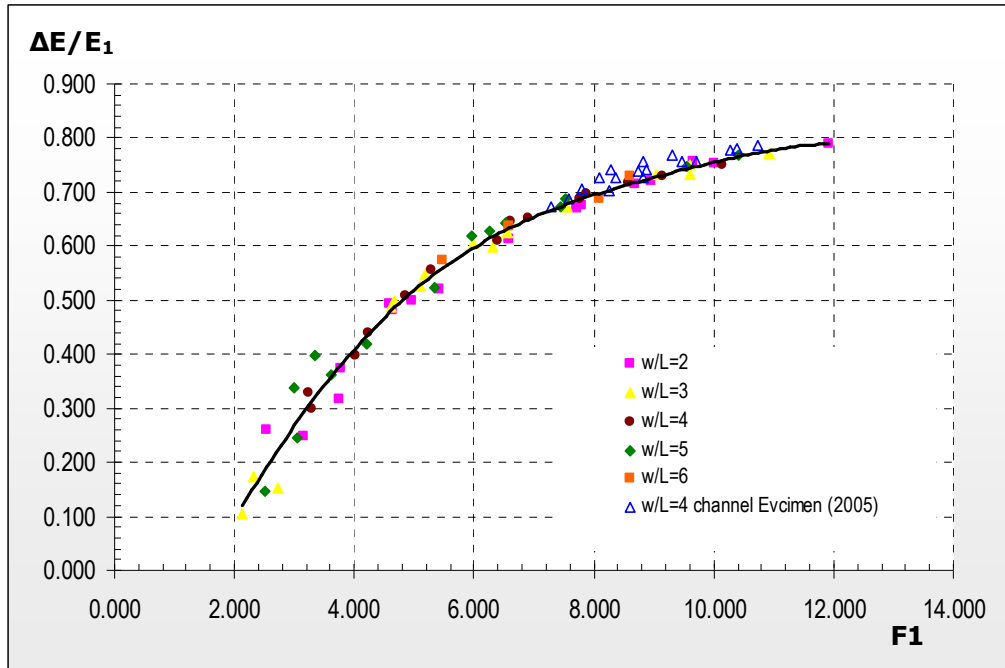


Figure 4.13: Energy dissipation with strip roughness versus F_1 for different length ratios

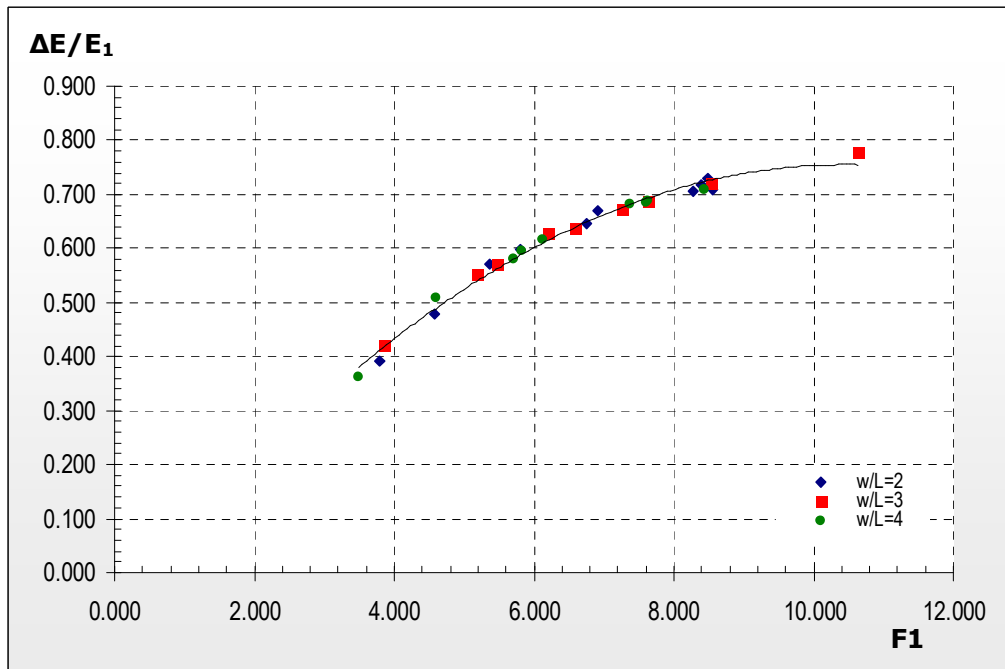


Figure 4.14: Energy dissipation rate for staggered roughness with respect to F_1

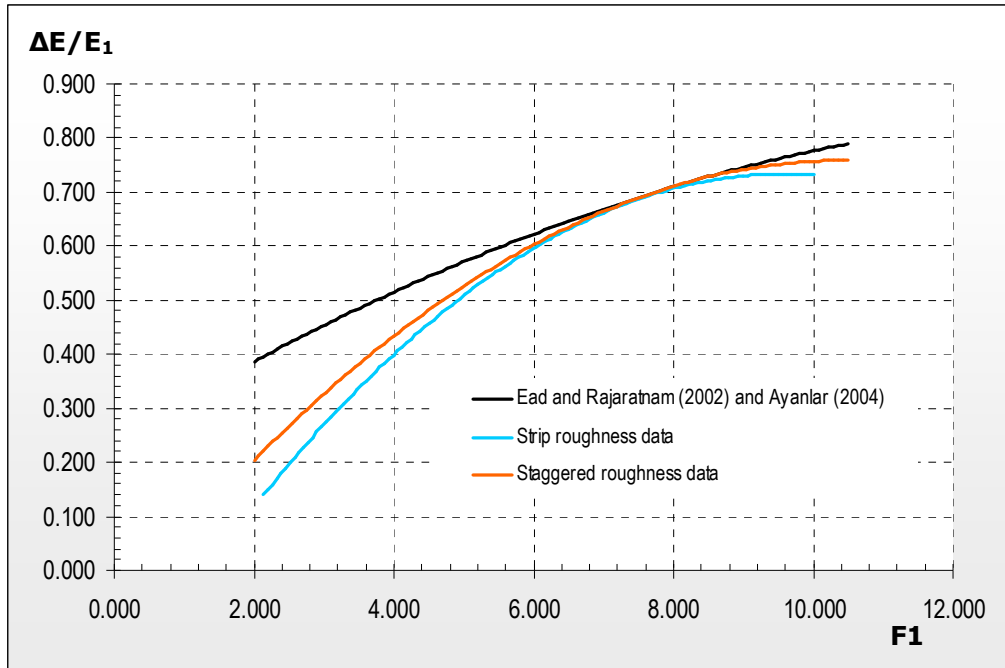


Figure 4.15: Comparison of the data obtained in this study with the previous ones

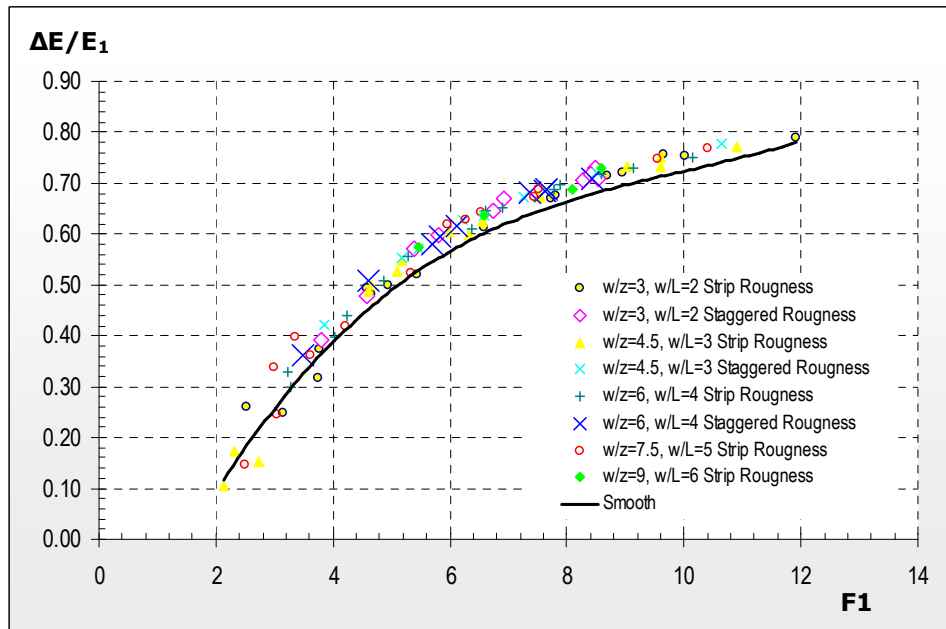


Figure 4.16: Energy dissipation rates in smooth channels and in channels with strip and staggered roughness versus F_1

Figure 4.16 illustrates the energy dissipation rates of strip and staggered roughness elements with different length and pitch ratios together with smooth beds. No significant influence of length and pitch ratios observed on the energy dissipation rate of a given flow. On the other hand, rough beds give slightly higher values of energy dissipation rate when compared with smooth beds.

4.4. Gain in Energy Dissipation

“Gain in energy dissipation” parameter can be defined as the percent of the additional dissipated energy by the roughness elements with regard to the energy dissipation of a smooth jump under identical upstream flow conditions. The parameter can be formulated as follows:

$$G_{ED} = \frac{\Delta E - \Delta E^*}{\Delta E} \times 100 \quad [4.3]$$

where,

ΔE is the energy loss for a jump formed in a rough bed

ΔE^* is the energy loss that would have been attained if a jump with the same supercritical flow parameters, y_1 and F_1 , had formed on a smooth bed [Equation 2.2]

The variation of percent gain in energy dissipation for varying length and pitch ratios and supercritical Froude numbers is presented in Figure 4.17. The gain in energy dissipation reduces with increasing supercritical Froude number for both strip and staggered roughness elements, which indicates that non-protruding roughness elements are getting less “felt” by the flow with increasing F_1 thus rough-bed characteristics converging to those of smooth bed.

Moreover, a trend line is drawn in order to depict the general behaviour of rough beds in terms of gain in energy dissipation in Figure 4.17. The dispersed data

points observed for Froude numbers lower than 4 falls outside the general tendency given by the trend line. Thus, these data points are omitted in sketching the trend line. The weak jump formation observed in cases for low Froude numbers should be the main reason of this discrepancy.

In the figure, one can see that the great majority of the data obtained in staggered roughness experiments lie over the trend line which indicates that more gain in energy loss is obtained with staggered roughness elements for tried cases.

From the trend line plotted, the following formula has been drawn:

$$G_{ED} = -0.5038 \times F_1 + 8.9337 \quad [4.4]$$

Equation 4.4 explains a relation between the gain in energy loss and varying incoming Froude number for flows on roughened beds.

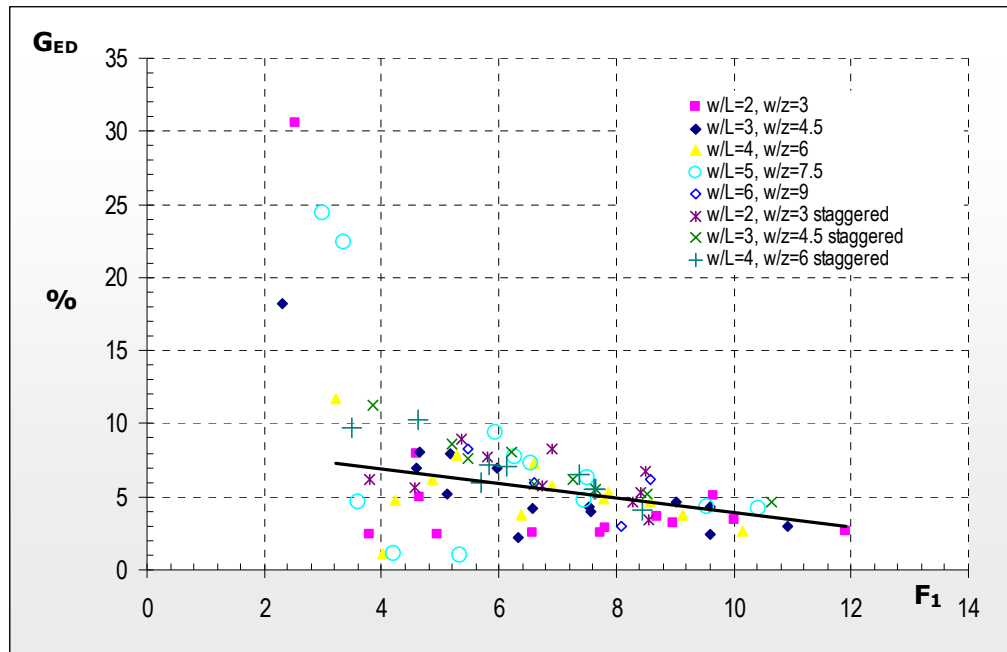


Figure 4.17: Percent gain in energy dissipation for different length and depth ratios for beds of strip and staggered roughness

4.5. Depth Ratio

Depth ratio is a ratio relating the subcritical depth, y_2 , to the supercritical depth, y_1 .

As illustrated in Section 2.3, length ratio, pitch ratio and lateral spacing parameter (staggered roughness arrangement in this study) may affect the depth ratio of a jump formed in a rough bed. Influence of length and pitch ratios on depth ratio is illustrated in Figure 4.18A for beds with strip roughness. No significant relation between the length and pitch ratios and variation of depth ratio for a given roughness arrangement could be observed from the figure.

However, the tailwater depth ratio for jumps in rough beds is smaller than that of jumps in smooth beds. The blue solid line for smooth beds and purple solid line for beds with strip roughness indicate that, as supercritical Froude number increases, more gain in depth ratio is obtained in beds with strip roughness compared to smooth beds.

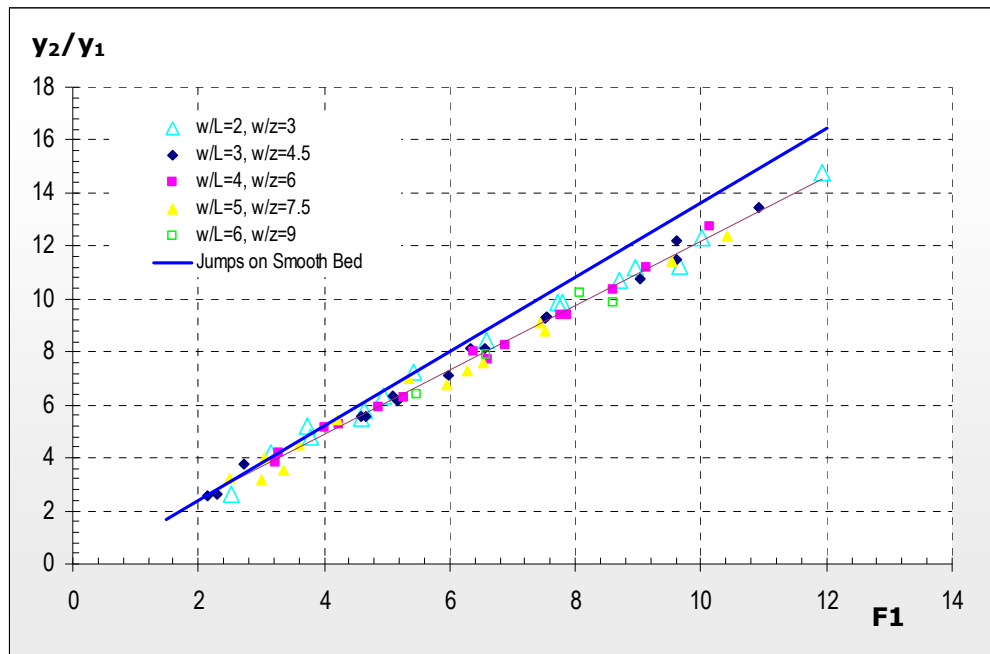


Figure 4.18A: Variation of depth ratio with supercritical Froude number for different length and pitch ratios in strip roughness arrangements

Both lines show that depth ratio is apt to increase with increasing incoming Froude number. Moreover, no significant relationship can be depicted with changing length and pitch ratio of a roughness arrangement and depth ratio of a jump on a bed with strip roughness.

On the other hand, Figure 4.18B shows the variation of depth ratio for flows over beds with staggered roughness elements. No significant deviation can be observed between the depth ratio trends of flows over staggered beds for different length and pitch ratios. The orange line for strip roughness gives slightly higher values of depth ratio compared to the black line for staggered roughness. Therefore, it can be concluded that staggered roughness arrangement proves a slightly better performance compared to strip roughness in terms of depth ratio. Both types illustrate a better performance compared to jumps formed on smooth beds.

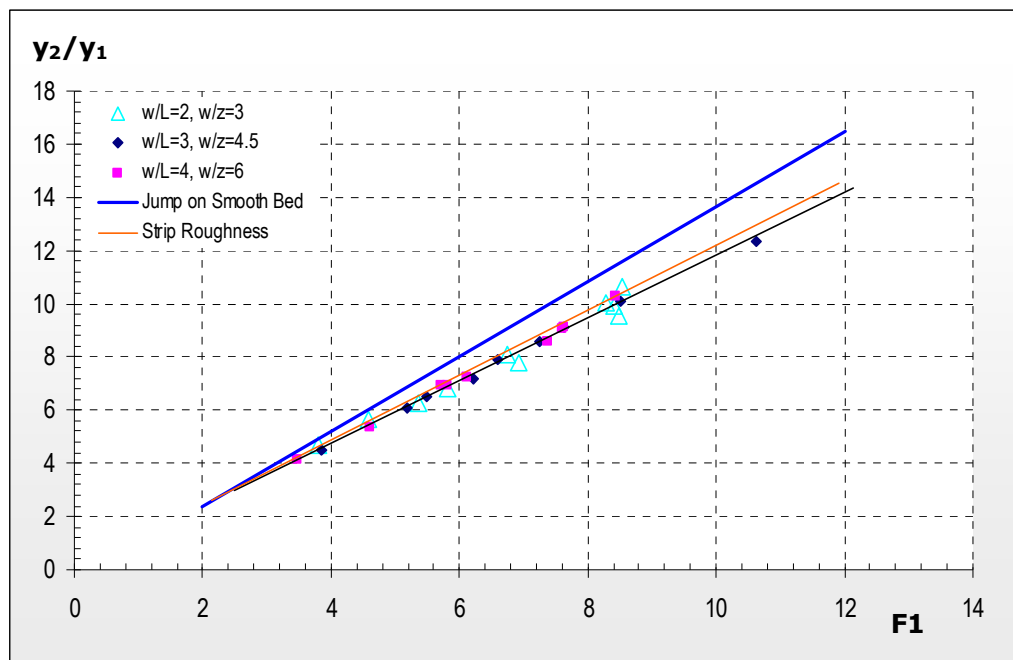


Figure 4.18B: Variation of depth ratio with supercritical Froude number for different length and pitch ratios in staggered roughness arrangements

While the positive effects of roughness elements on energy dissipation along the channel is given in the former sections of the text, those on jump length

reduction will be given in subsequent sections. When these significant positive effects are taken into consideration, one can conclude that a slight reduction in tailwater depth is a profit gained in advance.

4.6. Reduction in Tailwater Depth

Tailwater depth is an important parameter in a stilling basin design since its reduction will reduce the cost of the basin. To compare a jump formed in a rough bed with a smooth one, a percent depth reduction parameter may be formulated as introduced by Ead and Rajaratnam (2002):

$$D = \frac{y_2^* - y_2}{y_2^*} \times 100 \quad [4.5]$$

where,

y_2^* is the conjugate depth of the upstream flow depth, y_1

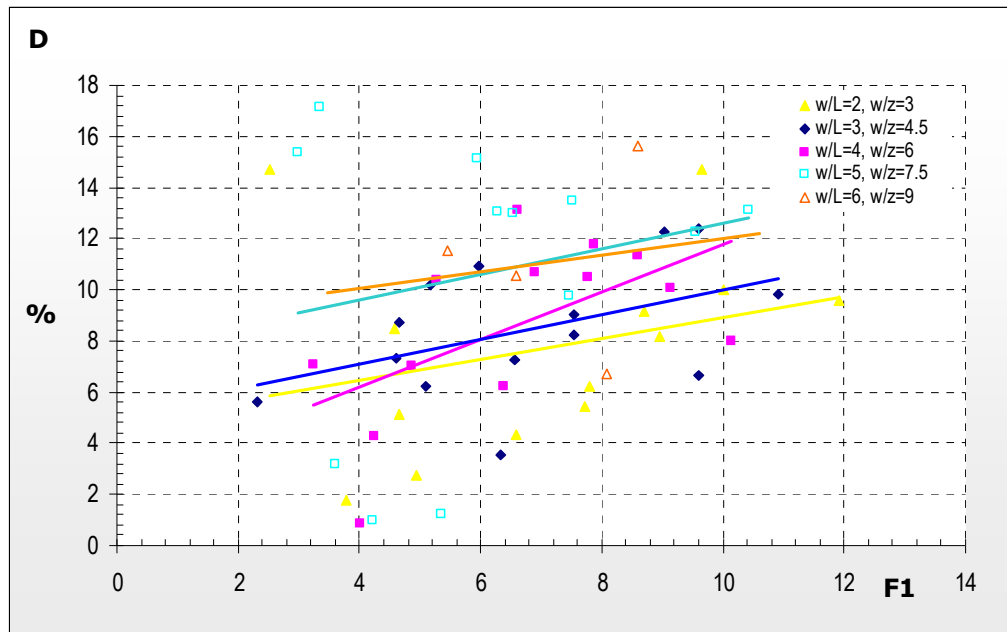


Figure 4.19A: Percent tailwater depth reduction in beds with strip roughness

Figure 4.19A illustrates that independent of length and pitch ratios of the roughness, increase in incoming Froude number brings about increase in the tailwater depth reduction in beds with strip roughness. Increase in length and pitch ratio seems to result in more reduction in tailwater depth as trend lines sketched in accordance with the colours of the regarding data points illustrate. However, the dispersed nature of the data points make this conclusion quite undependable. As the figure illustrates, on average, 5 to 13% reduction in tailwater depth is obtained in beds with strip roughness arrangement in the interval of F_1 values of 2 to 12.

The data gathered from staggered-roughness-arrangement experiments illustrate that staggered roughness gives a somewhat better performance compared to strip roughness arrangement. For Froude numbers in the range of 3-11, 7 to 15 percent reduction in tailwater depth is obtained in beds with staggered roughness with reference to tailwater depths of smooth jumps [Figure 4.19B]. Yet again, as F_1 increases, reduction in tailwater depth increases for all length and pitch ratios. However, the figure gives no meaningful conclusion about the relationship of length and pitch ratios and reduction in tailwater depth.

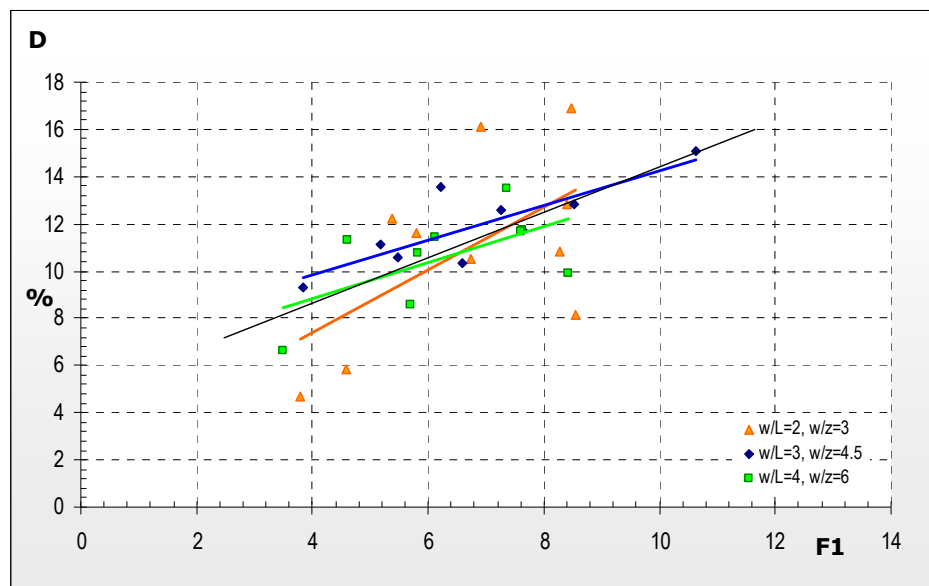


Figure 4.19B: Percent tailwater depth reduction in beds with staggered roughness

4.7. Length of Hydraulic Jump

Length of a hydraulic jump is another crucial parameter at the design stage of a stilling basin, since the length of the basin should be greater than the jump length in order to secure the overall structure against bed-scouring phenomenon.

In order to compare length of a jump formed in a rough bed with that of a smooth jump, conjugate depth of the upstream depth can be employed in the required comparison parameter. The dimensionless parameter, L_j/y_2^* , can be utilised to compare both.

As seen in Figure 4.20A, the ratio of length of jump to conjugate depth of supercritical depth reaches a constant value of 6.1 for Froude numbers greater than 5 in classical jumps as reported by USBR (1955). Beds with strip roughness present a better picture compared to smooth beds for upstream Froude numbers greater than 1.8. It can also be observed from the coloured solid lines drawn according to the related data points that as length and pitch ratios increase, jump-length parameter decreases slightly, which means sparser strip roughness arrangements produce slightly shorter jumps than the denser ones.

F_1 seems to have no significant effect on the jump length parameter defined here. As given by the dashed red line, the average value of the jump length for jumps on beds with strip roughness is $3.72y_2$, which is less than the two thirds of the classical jumps.

Some data points corresponding to low Froude numbers are excluded from data set illustrated in Figure 4.20A. These data give unpredictably high L_j/y_2^* values which falls outside expected tendency of proper data points. The principal reason for this consequence is the weak jump formation observed in runs with lower F_1 values especially when jump forms at the farther downstream of the sluice gate. The longitudinal distance of the jump-end for such cases is measured from the downstream section where the surface waves diminish, thus considerably increasing the jump length as illustrated in Figure 4.21.

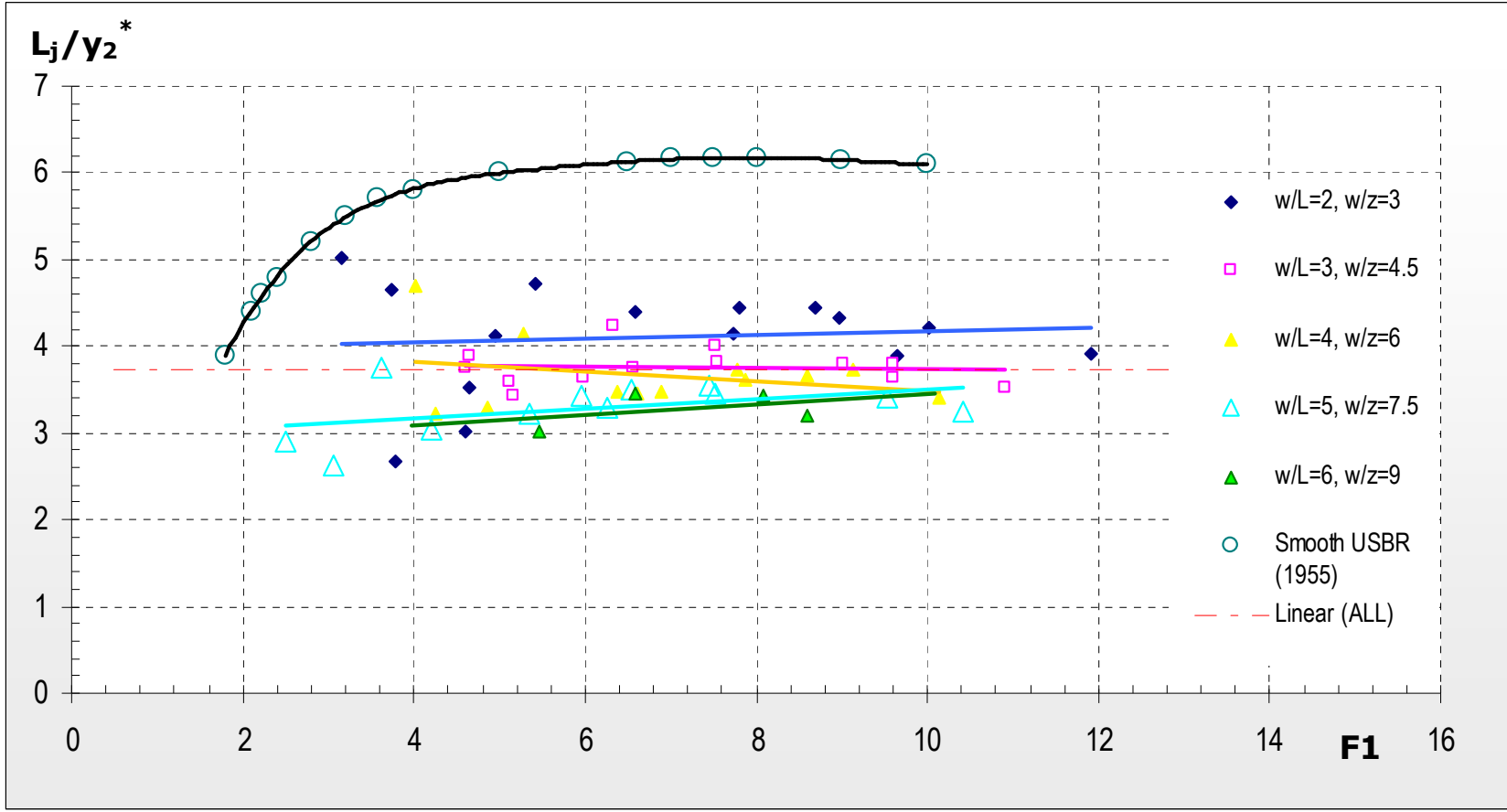


Figure 4.20A: L_j/y_2^* versus F_1 in beds with strip roughness

On the other hand, channels with non-protruding roughness elements in staggered arrangement produce jumps shorter than those in strip arrangement for F_1 values greater than 4.5. In Figure 4.20B, variation of jump-length parameter, L_j/y_2^* , is plotted versus incoming Froude number for flows on beds with staggered roughness elements of different length and pitch ratios. The colour of the solid trend lines is designated in accordance with the regarding data set. As given by the solid lines, no significant relation can be depicted between the length of jump and length and pitch ratios of staggered roughness elements.

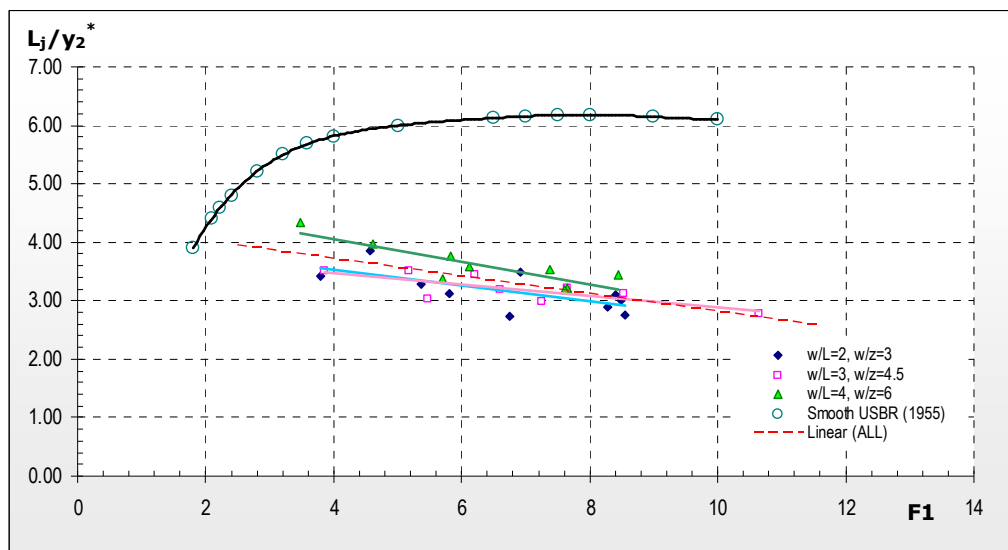


Figure 4.20B: L_j/y_2^* versus F_1 in beds with staggered roughness

In Figure 4.20B, it can be seen that as the incoming Froude number increases, the length of the jump decreases for all length and pitch ratios. When compared with the classical jump sketch given in the same figure, it is seen that with staggered roughness the length of the jump reduces to half of that observed on smooth beds around $F_1=8$.

In Figures 4.22A and 4.22B, the outline of the general performances of all smooth beds, beds with strip roughness and beds with staggered roughness are given independent of different length and pitch ratios.

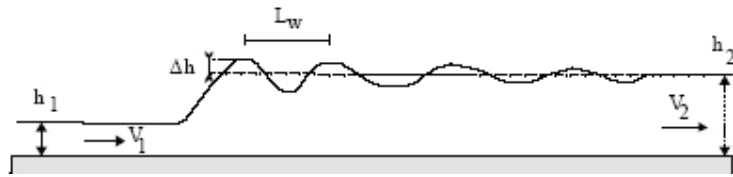


Figure 4.21: Sketch of an undular hydraulic jump (Chanson and Montes, 1995)

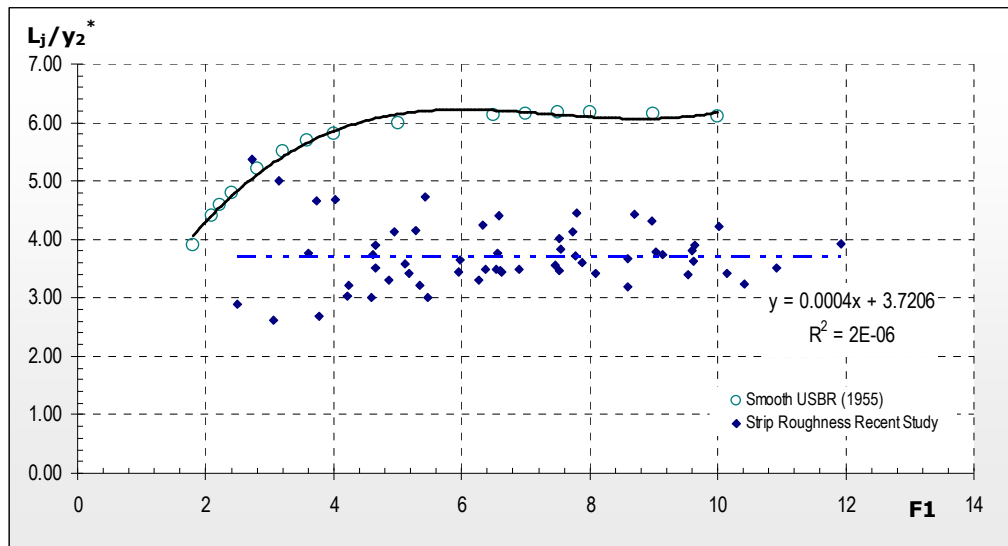


Figure 4.22A: Overall L_j/y_2^* trend for strip roughness

As seen in Figure 4.22A, when F_1 is greater than 3.5, a constant linear correlation is obtained between the jump-length parameter, L_j/y_2^* , and incoming Froude number values. The correlation with the incoming Froude number of the flow and jump-length parameter for beds with strip roughness can be given as:

$$\frac{L_j}{y_2^*} = 0.0004F_1 + 3.7206 \approx 3.72 \quad [4.6]$$

The formula of negatively sloped line converging to abscissa with increasing incoming Froude number for beds with staggered roughness is presented below:

$$\frac{L_j}{y_2^*} = -0.1504F_1 + 4.3108 \quad [4.7]$$

Solving Equations 4.6 and 4.7 simultaneously, one concludes that staggered roughness gives smaller jump length ratios than those of strip roughness for F_1 values greater than 3.9.

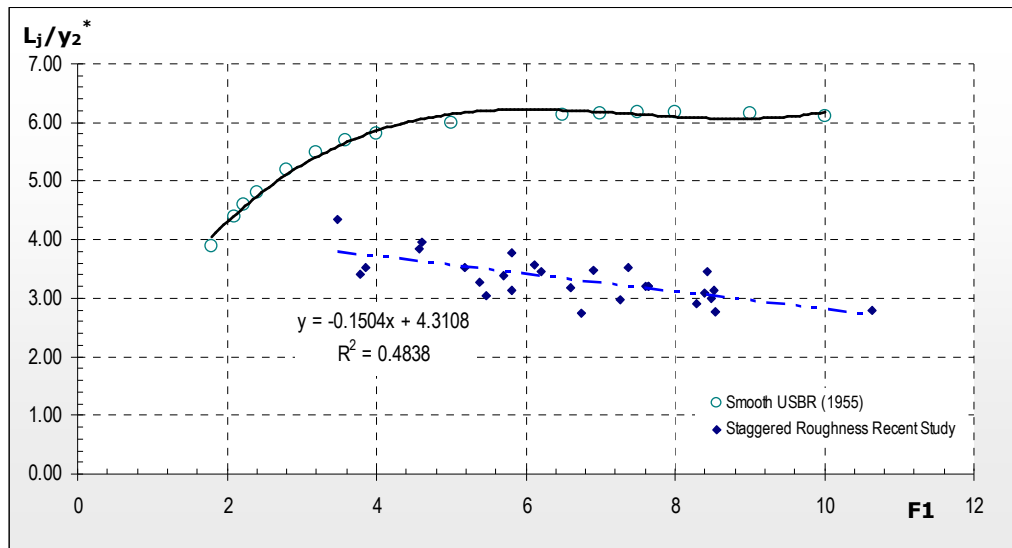


Figure 4.22B: Overall L_j/y_2^* trend for staggered roughness

4.8. Reduction in Length of Jump

The reduction in length of jump can be calculated by comparing the length of a jump on a rough bed with that that would be formed under identical upstream conditions in a smooth bed. Percent reduction in jump length may be defined as:

$$R_L = \frac{L_J^* - L_J}{L_J^*} \times 100 \quad [4.8]$$

where,

L_J is the length of jump formed in the rough bed

L_J^* is the length of jump that would be obtained in a smooth bed for identical upstream flow parameters, F_1 and y_1 , with the jump formed in the rough bed

In Figure 4.23A, the effect of varying length and pitch ratios on jump-length reduction factor versus upstream Froude number is presented. The solid trend lines are coloured in accordance with the data set they represent.

The reduction in the length of jump seems to be positively related with length and pitch ratios for strip roughness in the interval of $5 < F_1 < 10$. In other words, as strip roughness gets more dense, its capacity to reduce the length of jump decreases. Though different jump-length reduction versus F_1 tendencies observed for different length and pitch ratios, the overall trend depicted for strip roughness is constant around 40% as illustrated by the broken red line.

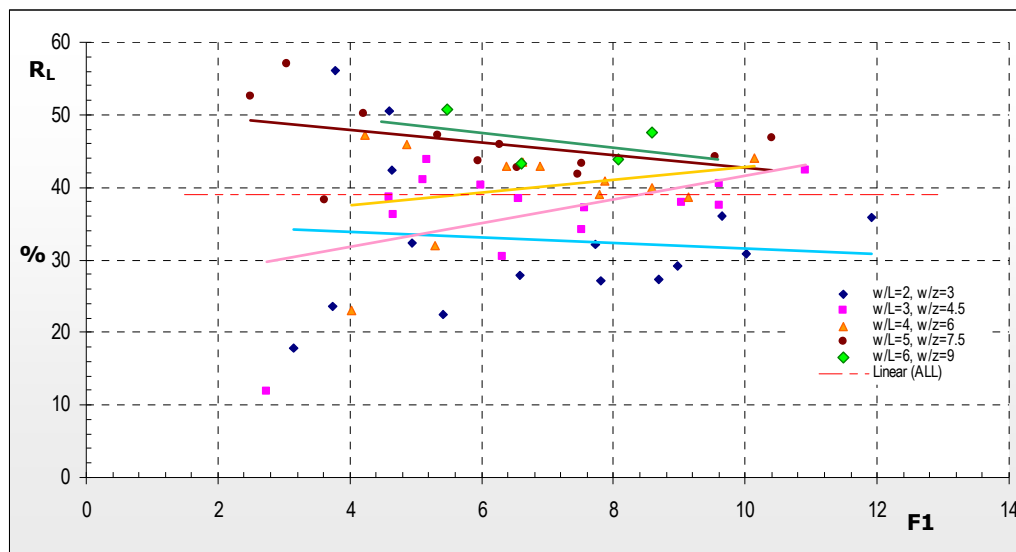


Figure 4.23A: Percent length reduction factor for strip roughness

Likewise, as reported by Ead and Rajaratnam (2002) and Ayanlar (2005), an increase in the pitch ratio brings about more reduction in jump-length for corrugated beds which is a consistent phenomenon with the effect of strip-roughness on hydraulic jump.

Once more, it should be remarked that the data obtained from jumps with lower F_1 values are omitted in Figure 4.23A. The fundamental reason lying beneath is that the weak jump formation encountered in such cases increases jump length leading to negative R_L values. Sorting out the weak jumps, a more explanatory correlation for each length and pitch ratio could be achieved.

Figure 4.23B illustrates the trends of jumps formed on beds with staggered roughness elements for varying F_1 values and different length and pitch ratios. No significant relation can be depicted between the length and pitch ratios of staggered roughness and rate of jump-length reduction as solid lines indicate.

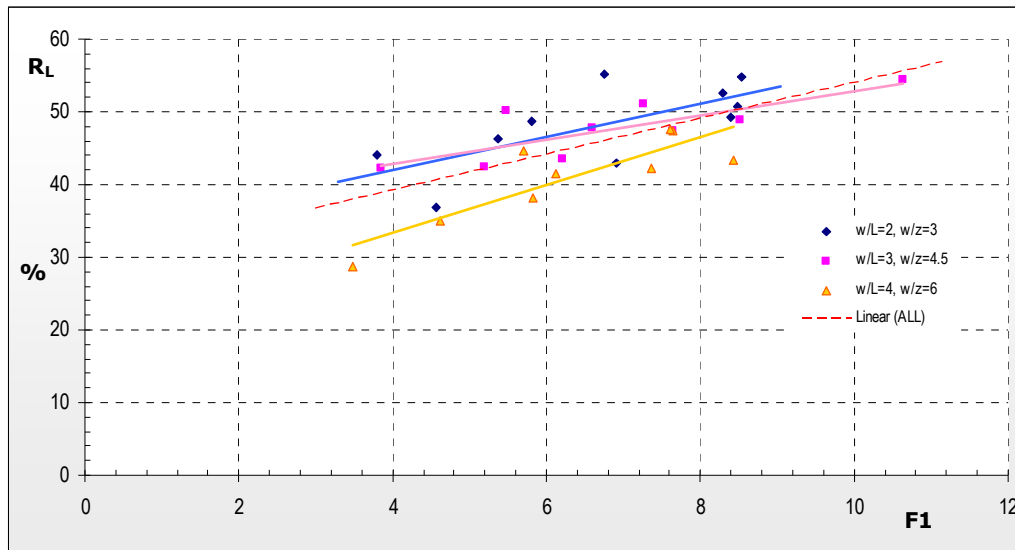


Figure 4.23B: Percent length reduction factor for staggered roughness

The broken red line, which gives the overall trend for staggered roughness in terms of jump length reduction, illustrates that as F_1 increases, reduction in the

length of jump increases too. Accordingly, staggered roughness results in 35 to 55% reduction in the length of jump for F_1 values in the interval of 4-10, when compared with smooth jumps.

CHAPTER V

CONCLUSIONS

5.1. Overall Assessment of Experimental Runs

In the present study, non-protruding strip- and staggered-roughness arrangements with different length and pitch ratios have been investigated to bring their effects on hydraulic jump characteristics into light in flows where supercritical Froude numbers vary between 2.13 and 11.92. Experiments were carried out in a rectangular sectioned laboratory flume with a horizontal bed. For the tests conducted for length ratios 2 to 11 and pitch ratios 3 to 16.5, the following conclusions are drawn:

1. The non-protruding roughness results in 3 to 7% more energy reduction than that obtained on smooth beds.
2. The gain in energy dissipation decreases as the upstream Froude number, F_1 , increases. In other words, flow is less likely to “feel” the effect of buried roughness.
3. Staggered roughness dissipates more energy compared to strip roughness.
4. Energy dissipation is basically a function of incoming Froude number. The length and pitch ratios of roughness do not have a significant effect on energy dissipation.
5. In artificially roughened beds, the tailwater depths are smaller than those of classical hydraulic jump on smooth beds. Strip roughness results in 5 to

13% tailwater depth reduction, whereas these values have risen up to 7 to 15% for staggered roughness.

6. The reduction in tailwater depth increases with increased Froude number.
7. The reduction in tailwater depth is independent of length and pitch ratios of the roughness for both strip and staggered roughness.
8. The jumps on beds with staggered roughness are more susceptible to tailwater depth variations. In some cases, this susceptibility eventually transformed the jump into a flow observed at the outlet of a flip bucket. Thus, strip roughness is a more dependable flow treatment utility for stilling basins.
9. Sparser roughness arrangements lead to shorter jump lengths with strip roughness.
10. For F_1 values exceeding 4, staggered roughness produces shorter jumps compared to strip roughness. However, no significant relation between the length and pitch ratio of roughness and jump length can be depicted.
11. Jump lengths for staggered roughness decrease with increasing F_1 .
12. Strip roughness results in 40% shorter jump lengths on average when compared to a classical jump with same supercritical conditions. On the other hand, this value increases with staggered roughness from 35 to 55% as F_1 increases from 4 to 10.
13. Staggered roughness produces slightly better results compared to strip roughness in terms of energy dissipation, tailwater depth reduction and jump length reduction. However, there arises an internal stability problem in the jump body, and it can easily transform to a flow with flip-bucket-like trajectory.

REFERENCES

- Abdelsalam, M. W., Elmongy, A., Abdellateef, M., Abouel-Atta, N. M., (1987), *Location and Length of Bed Roughness in Stilling Basins*, Scientific Bulletin, Vol. 1, No. 21, Faculty of Engineering, Ain Shams University, Cairo, Egypt, pp.288-312.
- Abdelsalam, M. W., Hammad, M. N., Elmongy, A., Mohamed Ali, H. S., (1985), *Effect of Length of Roughened Bed on Rectangular Hydraulic Jump*, Scientific Bulletin, Vol. 1, No. 16, Faculty of Engineering, Ain Shams University, Cairo, Egypt, pp. 263-297.
- Abdelsalam, M. W., Hammad, M. N., Khalifa, A., Abdellateef, M., (1986), *Roughened Bed Stilling Basin*, Scientific Bulletin, Vol. 1, No. 19, Faculty of Engineering, Ain Shams University, Cairo, Egypt, pp.178-198.
- Alhamid, A. A. and Negm, A. M., (1996), *Depth Ratio of Hydraulic Jump in Rectangular Stilling Basins*, Journal of Hydraulic Research, Vol. 34, No.5, pp. 597-604.
- Ayanlar, K., (2004), *Hydraulic Jump on Corrugated Beds*, M. Sc. Thesis, Middle East Technical University, Department of Civil Engineering, Ankara, Turkey.
- Bakhmeteff, B. A. and Matzke A. E., (1936), *The Hydraulic Jump in Terms of Dynamic Similarity*, Transactions, ASCE, Vol. 101, pp. 630-80.
- Bilgin, A., (2005), *Correlation and Distribution of Shear Stress for Turbulent Flow in a Smooth Rectangular Open Channel*, Journal of Hydraulic Research, Vol. 43, No. 2, pp. 165-173.
- Bradley, J. N. and Peterka, A. J., (1957), *The Hydraulic Design of Stilling Basins: Hydraulic Jumps on Horizontal apron (Basin I)*, Proc. ASCE, Jj. Hyd. Div., Vol 83, HY5, Paper No. 1410, pp.1-24, Discussions 1958, Paper 1616, 84 (HY2): pp.25-30, 1958 (HY5), Paper No. 1832, pp. 61-3.
- Celik, H. C., Birol, B., Gogus, M., (2003), *Effect of Roughness on Hydraulic Jump Properties*, I. National Hydraulic Engineering Symposium / Izmir, 22-26 September.

Chanson, H. and Brattberg, T., (2000), *Experimental Study of The Air-Water Shear Flow in a Hydraulic Jump*, International Journal of Multiphase Flow, 26, 583-607.

Chanson, H. and Montes, J. S., (1995), *Characteristics of Undular Hydraulic Jumps Experimental Apparatus and Flow Patterns*, Journal of Hydraulic Engineering, ASCE, Vol. 121, No. 2, pp. 129-144.

Chaurasia, S. R., (2003), *Direct Equations for Hydraulic Jump Elements in Rectangular Horizontal Channel*, Journal of Irrigation and Drainage Engineering, Vol. 129, ASCE, No. 4, August 1.

Chow, V. T., (1959), *Open Channel Hydraulics*, McGraw-Hill, New York.

Cui, J., Patel, V. C., Lin C-L, (2003), *Large-Eddy Simulation of Turbulent Flow in a Channel with Rib Roughness*, International Journal of Heat and Fluid Flow, 24, 372-88.

Ead, S. A. and Rajaratnam N., (2002), *Hydraulic Jumps on Corrugated Beds*, Journal of Hydraulic Engineering, ASCE, Vol. 128, No. 7, July 1.

Evcimen, T. U., (2005), *The Effect of Prismatic Roughness Elements on Hydraulic Jump*, M. Sc. Thesis, Middle East Technical University, Department of Civil Engineering, Ankara, Turkey.

Garimella, S. V. and Eibeck, P. A., (1992), *Fluid Dynamic Characteristics of the Flow over an Array of Large Roughness Elements*, InterSociety Conference on Thermal Phenomena.

Hager, W. H., (1990), *Geschichte des Wassersprungs* (in German), Schweiz Ing. Archit., 108(25), 728-35.

Hager, W. H., (1992), *Energy Dissipators and Hydraulic Jump*, Kluwer Academic Publishers, Dordrecht, The Netherlands.

Hager, W. H., (2003), *Forum: Alvin Peterka - Hydraulic Engineer*, Journal of Hydraulic Engineering, ASCE, September, 657-9.

Hager, W. H. and Bremen, R., (1989), *Classical Hydraulic Jump: Sequent Depths*, Journal of Hydraulic Res., 27 (5), 565-85.

Hákonardóttir, K. M., Hogg, A., Jóhannesson, T., (2003), *A Laboratory Study of the Interaction between Supercritical, Shallow Flows and Dams*, Vedustrofa Islands, Report No. 03038.

Hammad, M. N., Khalifa, A., Talaat, A. M., Abdellateef, M., Wafaie, E. M., (1988), *Optimum Height of Bed Roughness in Stilling Basins*, Scientific Bulletin of Faculty of Engineering, Ain Shams University, Cairo, Egypt, Vol. 1, No. 22, Civil Eng., pp. 59-73.

Harleman, D. R. F., (1959), *Discussion to Rouse et al.*, (1959), Trans. ASCE, Vol.124, pp. 959-62, (ed.) Hager, W. H. and Bremen, R., (1989), *Classical Hydraulic Jump: Sequent Depths*, Journal of Hydraulic Research, Vol. 27 (5), pp. 565-85.

Hughes, W. C. and Flack, J. E., (1983), *Hydraulic Jump Properties over a Rough Bed*, Journal of Hydraulic Engineering, ASCE, 110 (12), 1755-71.

Leutheusser, H. J. and Schiller, E.J., (1975), *Hydraulic Jump in a Rough Channel*, Int. Water Power and Dam Construction, Vol.27, No. 5, May, pp. 186-191.

Lin, C. H., Yen, J. F., Tsai, C. T., (2002), *Influence of Sluice Gate Contraction Coefficient on Distinguishing Condition*, Journal of Irrigation and Drainage Engineering, Vol. 128, No. 4, August 1.

Liu, M., Rajaratnam, N., Zhu, D. Z., (2004), *Turbulence Structure of Hydraulic Jumps of Low Froude Numbers*, Journal of Hydraulic Engineering, ASCE, June, 511- 19.

Krogstad, P. A. and Antonia, R. A., (1999), *Surface Roughness Effects in Turbulent Boundary Layers*, Experiments in Fluids, 27, Springer-Verlag, pp. 450-60.

Negm, A-A M., (2000), *Hydraulic Performance of Rectangular and Radial Stilling Basins*, 4th International Conference on Hydro-Science and -Engineering, Korea Water Resources Association, Korea.

Negm, A-A M., (2002), *Optimal Roughened Length of Prismatic Stilling Basins*, 5th International Conference on Hydro-Science and -Engineering, Warsaw.

Negm, A. M., Eisa, S. A., Waheed El-Din, U., (1993), *The Most Efficient Roughness Pattern for Dissipating the Energy Downstream Hydraulic Structures*, Proceedings of 1st Int. Conf. on Hydro-Science and Engineering (ICHE-'93), Vol. I, Advances in Hydro-Science and Engineering, Sam S.Y. Wang (Ed.), June 7-11, University of Mississippi, Washington, DC, USA, pp. 943-949.

Negm, A. M., Wafaie, E. M., Al-Othman, A. A., (1999), *Effect of Cube Roughness Height on The Performance of Stilling Basins*, Arab Gulf Journal of Scientific Research, Riyadh, Saudi Arabia, Vol. 17, No.1, pp. 35-47.

Mohamed Ali, H. S., (1991), *Effect of Roughened-Bed Stilling Basin on Length of Rectangular Hydraulic Jump*, Journal of Hydraulic Engineering, ASCE, JHEND8, Vol. 117, No. 1, p 83-93, January.

Montes, J. S., (1997), *Irrotational Flow and Real Fluid Effects under Planar Sluice Gates*, J. Hydraul. Eng., 123(3), 219-32.

Moore, W. L., (1943), *Energy Loss at the Base of a Free Overfall*, Transactions, ASCE, Vol. 108, pp. 1343-92.

Ohtsu, I. and Yasuda Y., (1994), *Characteristics of Supercritical Flow Below Sluice Gate*, Journal of Hydraulic Engineering, ASCE, Vol. 120, No. 3, March.

Ohtsu, I., Yasuda, Y., Awazu, S., (1990), *Free and Submerged Hydraulic Jump in Rectangular Channels*, Report No. 35, Res. Inst. of Sci. and Tech., Nihon Univ., Tokyo, Japan, 1-50.

Ohtsu, I., Yasuda, Y., Goto, H., (2003), *Flow Conditions of Undular Hydraulic Jumps in Horizontal Rectangular Channels*, Journal of Hydraulic Engineering, ASCE, Vol. 129, No. 12, December 1.

Perry, A. E., Schofield, W. H., Joubert, P. N., (1969), *Rough-Wall Turbulent Boundary Layers*, Journal of Fluid Mechanics, Vol. 37, pp. 383-413.

Peterka, A. J., (1953), *The Effect of Entrained Air on Cavitation Pitting*, 5th IAHR Congress, Minneapolis, 507-18.

Peterka, A. J., (1958), *Hydraulic Design of Stilling Basins and Energy Dissipators*, U.S. Bureau of Reclamation, Engineering Monograph, 25, U.S. Department of the Interior, Washington, D.C.

Rajaratnam, N., (1961), *Some Studies on the Hydraulic Jump*, Ph. D. Thesis, Indian Institute of Science, Bangalore, India.

Rajaratnam, N., (1962), *Profile Equation of the Hydraulic Jump*, Water Power, Vol. 14, August, pp. 324-7.

Rajaratnam, N., (1965), *The Hydraulic Jump as a Wall Jet*, J. Hydr. Div., ASCE, 91(5), 107-132.

Rajaratnam, N., (1967), *Hydraulic Jumps*, Advances in Hydrosience, Ven Te Chow, Ed., Vol. 4, Academic Press, New York, pp. 197-280.

Rajaratnam, N., (1968), *Hydraulic Jumps on Rough Beds*, Trans. Engineering Inst. of Canada, Vol. 11, No. A-2, pp. 1-8.

Rajaratnam, N., (1977), *Free flow immediately below sluice gates*, J. Hydr. Div., ASCE, 103(4), pp. 345-51.

Rajaratnam, N. and Hurtig, K. I. (2000), *Screen-Type Energy Dissipator for Hydraulic Structures*, Journal of Hydraulic Engineering, Vol. 126, No. 4, 310-12.

Rajaratnam, N. and Subramanya, K., (1968), *Profile of the Hydraulic Jump*, Journal of the Hydraulic Division, ASCE, Vol. 94, No. HY3, May.

Resch, F. J. and Leutheusser, H. J., (1972), *Le Ressaut Hydraulique: Mesure de Turbulence dans la Region Diphasique (The Hydraulic Jump: Turbulence Measurements in the Two-Phase Flow Region)* (in French), J. La Houille Blanche, (4), 279-93.

Streeter, V. L. and Wylie, E. B., (1981), *Fluid Mechanics*, McGraw-Hill, 1st SI Metric edition, Singapore.

Subramanya, K., (1986), *Flow in Open Channel*, Tata McGraw-Hill: New Delhi.

Tachie, M. F., Bergstrom, D. J., Balachandar, R., (2000), *Rough Wall Turbulent Boundary Layers in Shallow Open Channel Flow*, Journal of Fluids Engineering, September, Vol. 122, pp. 533-41.

Tani, I., (1987), *Turbulent Boundary Layer Development over Rough Surface*, Perspective in Turbulence Studies, Editor: Meier, H. U., Bradshaw, P., Springer-Verlag, pp. 223-49.

USBR, (1955), *Research Studies on Stilling Basins, Energy Dissipators and Associated Appurtenances*, US Bureau of Reclamation, Hydraulic Laboratory Report No. HYD-399.

APPENDIX A

COLLECTED AND COMPUTED DATA

TABLE AA: Tabular form of data collected in the present study

SET	STATUS	w cm	w/Z	w/L	H cm	Q l/s	y ₁ cm	y ₂ cm	F ₀	F ₁	F ₂	J _{start} cm	J _{end} cm
1	Strip	3	3	2	30.52	10.599	2.04	11.22	5.14	4.59	0.36	18.00	55.00
2	Strip	3	3	2	33.81	14.573	2.87	13.74	7.07	3.78	0.36	87.50	125.00
3	Strip	3	3	2	36.48	18.370	2.92	16.87	8.92	4.65	0.33	82.50	145.00
4	Strip	3	3	2	27.72	7.796	2.47	6.57	3.78	2.53	0.58	48.00	210.00
5	Strip	3	3	2	37.64	20.187	1.91	21.43	9.80	9.65	0.26	27.00	125.00
6	Strip	3	3	2	27.86	7.924	2.16	9.07	3.85	3.15	0.37	-3.10	40.00
7	Strip	3	3	2	30.40	10.468	2.32	12.05	5.08	3.74	0.32	-2.00	50.00
8	Strip	3	3	2	33.91	14.706	2.27	16.47	7.14	5.43	0.28	-2.20	75.00
9	Strip	3	3	2	36.51	18.416	2.07	20.48	8.94	7.80	0.25	-2.10	95.00
10	Strip	3	3	2	37.48	19.930	2.03	21.78	9.67	8.70	0.25	-1.30	105.00
11	Strip	3	3	2	27.88	7.942	1.60	10.15	6.45	4.95	0.31	2.45	45.50
12	Strip	3	3	2	30.48	10.555	1.60	13.50	8.57	6.58	0.27	-6.10	56.00
13	Strip	3	3	2	32.18	12.509	1.61	15.90	10.15	7.73	0.25	-0.40	69.20
14	Strip	3	3	2	33.66	14.375	1.60	17.90	11.67	8.96	0.24	-8.60	75.75
15	Strip	3	3	2	34.90	16.060	1.60	19.69	13.04	10.01	0.23	-4.90	87.45
16	Strip	3	3	2	35.80	17.353	1.50	22.20	14.09	11.92	0.21	-2.50	93.60
17	Staggered	3	3	2	27.75	7.823	1.50	9.37	6.81	5.37	0.34	-7.90	27.10
18	Staggered	3	3	2	30.40	10.468	1.54	12.00	9.11	6.91	0.32	-11.35	38.40
19	Staggered	3	3	2	32.05	12.353	1.50	14.35	10.75	8.49	0.29	-8.00	43.90
20	Staggered	3	3	2	33.60	14.296	1.68	16.82	12.44	8.29	0.26	-7.70	46.95
21	Staggered	3	3	2	27.80	7.869	1.90	8.85	3.82	3.79	0.38	-9.70	22.00
22	Staggered	3	3	2	30.20	10.252	2.00	11.28	4.98	4.57	0.34	-8.15	38.00
23	Staggered	3	3	2	32.20	12.533	1.95	13.32	6.08	5.81	0.33	-4.70	42.40

SET	STATUS	w cm	w/Z	w/L	H cm	Q l/s	y ₁ cm	y ₂ cm	F ₀	F ₁	F ₂	J _{start} cm	J _{end} cm
24	Staggered	3	3	2	33.80	14.560	1.95	15.80	7.07	6.75	0.29	2.00	50.35
25	Staggered	3	3	2	35.20	16.484	1.83	18.17	8.00	8.40	0.27	-11.30	53.30
26	Staggered	3	3	2	36.15	17.872	1.91	20.34	8.67	8.54	0.25	-0.55	60.60
27	Strip	4.5	4.5	3	30.40	10.468	3.20	8.46	5.08	2.31	0.54	57.55	200.00
28	Strip	4.5	4.5	3	34.02	14.853	2.53	14.10	7.21	4.66	0.35	34.90	95.00
29	Strip	4.5	4.5	3	36.50	18.401	2.47	17.55	8.93	5.98	0.32	33.20	105.00
30	Strip	4.5	4.5	3	37.47	19.914	2.87	17.60	9.66	5.17	0.34	62.88	130.00
31	Strip	4.5	4.5	3	27.99	8.044	2.83	7.34	3.90	2.13	0.51	29.60	180.00
32	Strip	4.5	4.5	3	30.40	10.468	2.02	11.28	5.08	4.60	0.35	4.40	50.00
33	Strip	4.5	4.5	3	34.15	15.027	2.08	16.96	7.29	6.32	0.27	-4.50	70.00
34	Strip	4.5	4.5	3	36.51	18.416	2.12	19.59	8.94	7.53	0.27	-1.50	85.00
35	Strip	4.5	4.5	3	37.48	19.930	1.98	21.33	9.67	9.03	0.26	2.90	95.00
36	Strip	4.5	4.5	3	27.89	7.952	2.38	8.93	3.86	2.73	0.38	-3.50	40.00
37	Strip	4.5	4.5	3	27.90	7.961	1.57	9.92	6.46	5.11	0.32	-1.15	36.85
38	Strip	4.5	4.5	3	30.45	10.522	1.60	13.05	8.54	6.56	0.28	1.75	54.55
39	Strip	4.5	4.5	3	32.04	12.341	1.62	15.15	10.02	7.55	0.26	-9.10	54.20
40	Strip	4.5	4.5	3	33.58	14.270	1.52	17.45	11.58	9.61	0.25	-3.50	68.80
41	Strip	4.5	4.5	3	34.95	16.130	1.65	20.17	13.09	9.60	0.22	-2.70	79.60
42	Strip	4.5	4.5	3	35.90	17.501	1.60	21.55	14.21	10.91	0.22	-3.20	80.80
43	Staggered	4.5	4.5	3	27.87	7.933	1.89	8.52	3.85	3.85	0.40	-7.00	26.10
44	Staggered	4.5	4.5	3	30.05	10.092	1.82	11.08	4.90	5.19	0.35	-6.42	37.40
45	Staggered	4.5	4.5	3	32.32	12.679	1.88	13.48	6.15	6.21	0.32	-7.60	46.10
46	Staggered	4.5	4.5	3	33.88	14.666	1.99	15.77	7.12	6.59	0.30	-7.72	48.34
47	Staggered	4.5	4.5	3	35.20	16.484	1.95	17.75	8.00	7.64	0.28	-11.15	53.40
48	Staggered	4.5	4.5	3	27.74	7.814	1.48	9.61	6.80	5.48	0.33	-7.60	25.00
49	Staggered	4.5	4.5	3	30.49	10.566	1.50	12.82	9.20	7.26	0.29	-11.30	32.40
50	Staggered	4.5	4.5	3	31.99	12.281	1.49	15.02	10.69	8.52	0.27	-10.30	43.50
51	Staggered	4.5	4.5	3	33.46	14.114	1.41	17.43	12.28	10.64	0.24	-11.35	45.70
52	Strip	6	6	4	30.39	10.457	2.53	10.55	5.07	3.28	0.39	19.20	105.00
53	Strip	6	6	4	34.00	14.826	2.69	14.21	7.19	4.24	0.35	47.20	95.00
54	Strip	6	6	4	36.45	18.325	2.83	16.81	8.89	4.86	0.34	45.30	105.00
55	Strip	6	6	4	37.40	19.803	2.16	20.28	9.61	7.87	0.27	1.95	85.00
56	Strip	6	6	4	28.20	8.240	2.18	8.30	4.00	3.23	0.43	17.15	135.00
57	Strip	6	6	4	34.00	14.826	2.00	15.41	7.19	6.61	0.31	8.90	70.00
58	Strip	6	6	4	36.53	18.447	2.37	18.97	8.95	6.38	0.28	4.45	75.00
59	Strip	6	6	4	30.40	10.468	2.21	11.41	5.08	4.02	0.34	-4.00	50.00

SET	STATUS	w cm	w/Z	w/L	H cm	Q l/s	y ₁ cm	y ₂ cm	F ₀	F ₁	F ₂	J _{start} cm	J _{end} cm
60	Strip	6	6	4	28.28	8.315	1.58	9.90	6.75	5.28	0.34	-6.50	39.30
61	Strip	6	6	4	30.56	10.643	1.56	12.90	8.64	6.89	0.29	0.90	51.15
62	Strip	6	6	4	32.15	12.473	1.60	15.05	10.12	7.78	0.27	-5.60	57.00
63	Strip	6	6	4	33.70	14.428	1.65	17.05	11.71	8.59	0.26	-4.50	66.00
64	Strip	6	6	4	34.90	16.060	1.70	19.02	13.04	9.14	0.24	-9.70	69.35
65	Strip	6	6	4	35.80	17.353	1.67	21.30	14.09	10.15	0.22	-6.10	72.85
66	Staggered	6	6	4	32.30	12.655	1.96	13.55	5.86	5.82	0.32	-12.55	44.70
67	Staggered	6	6	4	33.88	14.666	2.09	15.14	6.79	6.13	0.31	-5.85	55.15
68	Staggered	6	6	4	35.20	16.484	1.95	17.75	7.63	7.64	0.28	-11.15	53.40
69	Staggered	6	6	4	36.30	18.098	2.08	18.88	8.37	7.61	0.28	-4.00	64.40
70	Staggered	6	6	4	27.83	7.896	1.45	10.06	6.87	5.71	0.31	-12.70	24.50
71	Staggered	6	6	4	30.44	10.511	1.48	12.71	9.15	7.37	0.29	-11.00	40.85
72	Staggered	6	6	4	31.99	12.281	1.50	15.46	10.69	8.44	0.25	-14.90	44.35
73	Staggered	6	6	4	27.80	7.869	2.01	8.36	3.64	3.48	0.41	-9.25	29.65
74	Staggered	6	6	4	30.35	10.414	2.01	10.77	4.82	4.61	0.37	-10.10	38.02
75	Strip	7.5	7.5	5	30.62	10.709	2.73	8.70	5.20	3.00	0.53	36.35	150.00
76	Strip	7.5	7.5	5	33.75	14.494	3.77	12.13	7.03	2.50	0.43	61.50	95.00
77	Strip	7.5	7.5	5	36.47	18.355	3.86	15.37	8.91	3.05	0.38	76.00	115.00
78	Strip	7.5	7.5	5	37.36	19.739	3.27	17.74	9.58	4.21	0.33	50.60	105.00
79	Strip	7.5	7.5	5	27.79	7.860	2.06	7.29	3.81	3.35	0.50	11.75	170.00
80	Strip	7.5	7.5	5	27.79	7.860	1.96	8.80	3.81	3.61	0.38	-13.40	20.80
81	Strip	7.5	7.5	5	30.39	10.457	1.70	11.45	5.07	5.95	0.34	-10.10	36.20
82	Strip	7.5	7.5	5	36.58	18.523	2.13	18.70	8.99	7.52	0.29	1.10	75.80
83	Strip	7.5	7.5	5	33.98	14.799	2.07	15.09	7.18	6.27	0.32	6.50	63.70
84	Strip	7.5	7.5	5	37.48	19.930	2.25	20.40	9.67	7.45	0.27	1.35	81.75
85	Strip	7.5	7.5	5	27.70	7.778	1.50	10.48	6.31	5.34	0.29	-5.65	28.50
86	Strip	7.5	7.5	5	30.41	10.479	1.60	12.19	8.51	6.53	0.31	-2.70	46.20
87	Strip	7.5	7.5	5	33.50	14.166	1.52	17.34	11.50	9.54	0.25	-12.40	54.75
88	Strip	7.5	7.5	5	35.89	17.486	1.65	20.40	14.19	10.41	0.24	-4.10	72.00
89	Strip	9	9	6	27.90	7.961	1.50	9.62	6.46	5.47	0.34	-12.00	20.70
90	Strip	9	9	6	30.50	10.577	1.60	12.65	8.59	6.60	0.30	-5.00	44.00
91	Strip	9	9	6	32.18	12.509	1.50	14.76	10.15	8.59	0.28	-4.00	52.00
92	Strip	9	9	6	33.52	14.192	1.70	17.35	11.52	8.08	0.25	-10.85	52.80

APPENDIX B

FORMER EMPIRICAL WORK

TABLE BA: Evcimen's data for $w/Z=4$ and $w/Z=6.67$ (Evcimen, 2005)

SET	w cm	w/Z	H cm	Q l/s	y ₁ cm	y ₂ cm	F ₁	F ₂	J _{start} cm	J _{end} cm
58	4	6.67	35.70	14.036	1.30	17.48	11.95	0.24	56.00	126.00
59	4	6.67	35.70	14.036	1.29	17.24	12.09	0.25	12.00	96.00
60	4	6.67	37.50	16.484	1.29	21.13	14.20	0.21	12.00	109.00
61	4	6.67	38.99	18.692	1.30	23.46	15.91	0.21	11.00	113.00
62	4	6.67	38.99	18.692	1.34	22.37	15.21	0.22	96.00	181.00
63	4	6.67	38.99	18.692	1.35	22.38	15.04	0.22	72.00	168.00
64	4	6.67	38.49	17.933	1.29	21.54	15.45	0.23	16.00	113.00
65	4	6.67	39.21	19.032	1.76	20.54	10.29	0.26	81.00	177.00
66	4	6.67	39.21	19.032	1.71	20.67	10.74	0.26	29.00	107.00
67	4	6.67	39.21	19.032	1.75	20.41	10.37	0.26	63.00	148.00
68	4	6.67	37.69	16.757	1.71	18.38	9.46	0.27	17.00	106.00
69	4	6.67	37.69	16.757	1.68	18.96	9.71	0.26	32.00	117.00
70	4	6.67	37.69	16.757	1.73	16.99	9.29	0.30	72.00	146.00
71	4	6.67	36.98	15.753	1.72	18.22	8.81	0.26	48.00	117.00
72	4	6.67	36.15	14.626	1.71	17.23	8.25	0.26	22.00	98.00
73	4	6.67	37.75	16.843	2.04	17.79	7.29	0.28	62.00	128.00
74	4	6.67	37.75	16.843	1.99	17.69	7.57	0.29	26.00	98.00
75	4	6.67	37.75	16.843	1.95	17.22	7.81	0.30	13.00	93.00
76	4	6.67	39.38	19.297	1.98	19.45	8.74	0.28	56.00	144.00
77	4	6.67	39.38	19.297	1.96	19.78	8.87	0.28	24.00	117.00
78	4	6.67	39.38	19.297	1.97	18.22	8.81	0.31	12.00	108.00
79	4	6.67	38.46	17.888	1.98	17.45	8.10	0.31	58.00	137.00

SET	w cm	w/Z	H cm	Q l/s	y ₁ cm	y ₂ cm	F ₁	F ₂	J _{start} cm	J _{end} cm
80	4	6.67	38.46	17.888	1.95	16.98	8.29	0.32	19.00	102.00
81	4	6.67	38.46	17.888	1.94	18.28	8.35	0.29	9.00	96.00
1	4	4	32.95	10.523	1.11	14.75	11.35	0.23	157.00	226.00
2	4	4	32.86	10.425	1.07	15.20	11.89	0.22	93.00	154.00
3	4	4	34.00	11.704	1.08	17.08	13.16	0.21	127.00	196.00
4	4	4	34.00	11.704	1.08	16.60	13.16	0.22	78.00	156.00
5	4	4	35.56	13.600	1.33	17.79	11.19	0.23	78.00	153.00
6	4	4	36.63	15.001	1.35	19.00	12.07	0.23	102.00	178.00
7	4	4	37.53	16.243	1.38	20.06	12.64	0.23	145.00	224.00
8	4	4	34.55	12.353	1.37	14.87	9.72	0.27	106.00	167.00
9	4	4	32.95	10.523	1.34	14.02	8.56	0.25	63.00	117.00
10	4	4	35.70	13.779	1.37	17.43	10.84	0.24	130.00	204.00

TABLE BB: Ayanlar's data for t=10 (Ayanlar, 2004)

SET	Q l/s	y ₁ cm	y ₂ cm	F ₁	J _{start} cm	L _j cm
5	9.418	1.17	13.20	9.45	55.00	70.00
6	9.418	1.15	13.41	9.64	20.00	70.00
7	11.157	1.18	13.80	11.05	95.00	80.00
8	11.157	1.27	15.22	9.84	65.00	85.00
9	11.426	1.55	12.72	7.47	55.00	72.00
10	11.426	1.65	14.02	6.80	25.00	65.00
22	7.286	1.05	10.89	8.55	20.00	45.00
23	5.720	0.92	9.27	8.18	15.00	41.00
44	10.672	1.36	13.39	8.49	0.00	80.00
45	13.892	1.30	17.45	11.83	5.00	90.00

TABLE BC: Data of Ead and Rajaratnam for $t=1.3$ and $t=2.2$ (Ead and Rajaratnam, 2002)

SET	t cm	q m ² /s	y ₁ cm	y ₂ cm	F ₁	L _j cm
A1	1.3	0.051	2.54	10.40	4.00	41.00
A2	1.3	0.063	2.54	12.80	5.00	48.00
A3	1.3	0.076	2.54	14.50	6.00	54.00
A4	1.3	0.089	2.54	18.80	7.00	75.00
A5	1.3	0.101	2.54	20.00	8.00	85.00
A6	1.3	0.114	2.54	23.30	9.00	102.00
A7	1.3	0.127	2.54	26.30	10.00	109.00
B1	1.3	0.143	5.08	21.00	4.00	88.00
B1	1.3	0.207	5.08	31.00	5.80	129.00
C1	2.2	0.143	5.08	21.00	4.00	82.00
C2	2.2	0.207	5.08	31.00	5.80	129.00

TABLE BD: Data of USBR for length parameter (USBR, 1955)

F ₁	L _j
1.80	3.90
2.10	4.40
2.22	4.60
2.4	4.80
2.80	5.20
3.20	5.50
3.58	5.70
4.00	5.80
5.00	6.00
6.50	6.13
7.00	6.16
7.50	6.17
8.00	6.18
9.00	6.15
10.00	6.10

APPENDIX C

LABCARD MANAGEMENT AND PROBE CALIBRATION

The following text is taken from the web page <http://www.churchill-controls.co.uk/downloads/wmman.pdf> in order to set up and use the Labcard in the Hydromechanics Laboratory at METU prior to experimental stage of this study. Since necessary documentation is not accessible in the Laboratory, the following text will certainly be helpful for prospective researchers and Labcard users and in new studies. As a final remark, it should be reminded to new researchers that the software "470.exe" should be run in DOS operating system on the computer in the Hydromechanics Laboratory at METU in order to take the digitalised output of the analog data sent by the Labcard.

There are two settings, one for the frequency and one for sensitivity made on the circuit card. For these the module must be withdrawn from the case.

FREQUENCY SELECTION

The energisation frequency of the probe is selected by inserting a jumper into one of a series of 6 card mounted pins. Each pin is labelled with the approximate frequency. When probe are used in close proximity to each other there is some advantage in operating the probe at the highest frequency to reduce the ripple content of the output signal.

SENSITIVITY SWITCH

The small jumper mounted in the circuit board alters the amplitude of the energisation voltage which is applied to the SET DATUM control. For probes up to 500mm in length the jumper should be set to position "S", i.e. with its jumper moved towards the front panel. For longer probes the jumper should be set to position "L", i.e. towards the rear plug connector to reduce the sensitivity of the SET DATUM control.

CONNECTION OF PROBE

The probe may be connected either to the red 4 mm sockets on the front panel by means of the plugs provided, or by means of terminal connections at the back. The connecting cable should be a twisted pair or a flat "figure 8". No special characteristics are required and a suitable cable would be one consisting of 2 conductors each 7/0.25mm (2 amp). The energisation voltage is balanced about earth so it is important that neither of the conductors is earthed.

LEAD COMPENSATION

The instrument incorporates means for compensation for the resistance of the connecting cable to ensure that a high degree of linearity of measurements is maintained over a very wide dynamic range of probe conductivity. Disconnect the probe cable at the probe end and insert the plugs into the blue TEST sockets on the front panel. Depress the toggle switch into the TEST position, turn the SET OUTPUT control to its fully clockwise position, (i.e. maximum) and adjust the SET DATUM control until the pointer of the balance meter is in its central position (rotating the control clockwise raises the meter pointer). Depress the push button and rotate the COMP control with a screwdriver to restore the pointer to its balance position. Correct compensation is achieved when pressing and releasing the push-button results in no change in the position of the meter pointer. The plugs can then be removed from the TEST sockets and reconnected to the probe.

OUTPUT SIGNALS

The instrument provides an output signal with a centre zero at earth potential and with maximum excursions of + and - 10 volts. Connections can be made either to the OUTPUT coaxial plug on the front panel or by terminal connections at the rear where the following signals are available:-

Terminal 1: 10V; 0; -10V

Terminal 2: 10mA; 0; - 10mA from a source impedance of 1 K ohm.

Terminal 3: 0.05 mA; -0.05 mA with a parallel resistance of 240 ohms for galvanometer recorder. (Galvo. SMI/S).

The frequency response of the output signals is limited by the smoothing filter in the rectifier circuit which has a 95% response at 10Hz.

SET DATUM

This enables the output signal to be set to zero, i.e. to earth potential, for any initial depth of probe immersion. The instrument will then give its maximum full scale output of + and - 10 volts for waves which just reach the bottom of the probe in their troughs. To set up the control, fix the probe in position immersed to the required depth in still water, set the toggle switch on the front panel to the OPERATE position, set the SET OUTPUT control to its fully clockwise position, and then rotate the SET DATUM control to bring the indicating meter to its central position.

SET OUTPUT

This control attenuates the output signal and enables it to be set for a maximum voltage of any value between zero and 10 volts. Provided the datum has been adjusted as described in the previous paragraph the dial calibrations read directly in volts and/or milliamps. All that is required is to set the dial to required output and to lock it. Note that in doing so, the sensitivity of the datum adjustment and the cable resistance compensation described above is reduced, and it is recommended that this control always be set to its maximum before carrying out these operations.